Received: 23 August 2024 | Revised: 20 March 2025 | Accepted: 18 April 2025

DOI: 10.1111/bph.70075

RESEARCH ARTICLE

Casdatifan (AB521) is a novel and potent allosteric small molecule inhibitor of protumourigenic HIF-2α dependent transcription

Patrick G. Schweickert | Dana Piovesan | Casey G. Mitchell | Bryan Zepeda-Carranza | Wandi S. Zhu | Alejandra Y. Lopez Espinoza | Lauren Rocha | Jaskirat Singh | Martin Ian P. Malgapo | Cesar Meleza | Kyle R. Northington | Rebecca D. Ray | Xiaoning Zhao | Kenneth V. Lawson | Matthew J. Walters | Kelsey E. Sivick

Arcus Biosciences Inc, Hayward, California, USA

Correspondence
Kelsey E. Sivick, Arcus Biosciences Inc., 3928 Point Eden Way, Hayward, CA 94545, USA.
Email: ksivick@arcusbio.com

Funding information
Arcus Biosciences, Inc.

Abstract

Background and Purpose: Hypoxia-inducible factor 2α (HIF-2α) is a transcription factor that mediates the expression of genes critical for cell adaptation and survival in low oxygen (hypoxic) conditions. In cancer, hypoxic conditions or molecular alterations within cancer cells can lead to HIF-2α accumulation and promote tumour growth and progression. Inactivating mutations in the von Hippel–Lindau (*VHL*) gene disable the oxygen-dependent HIF-2α degradation pathway and cause constitutive HIF-2α activity. *VHL* mutations are prevalent in clear cell renal cell carcinoma (ccRCC) where HIF-2α is a known tumourigenic driver. HIF-2α inhibition was shown to improve ccRCC patient outcomes clinically, warranting development of next-generation inhibitors.

Experimental Approach: Pharmacological effects of a novel small molecule allosteric inhibitor of HIF-2α, AB521 (casdatifan), were evaluated using in vitro cell-based assays and in vivo mouse models.

Key Results: AB521 inhibited HIF-2α-mediated transcription in cancer cells, endothelial cells, and M2-polarised macrophages. AB521 was selective for HIF-2α, displaying no activity against HIF-1α, and did not exhibit off-target cytotoxicity. When delivered orally to mice, AB521 caused dose-dependent decreases in HIF-2α-associated pharmacodynamic markers and significant regression of human ccRCC xenograft tumours. AB521 combined favourably with cabozantinib, a standard of care tyrosine kinase inhibitor, or zimberelimab, a clinical-stage anti-PD-1 antibody, in ccRCC xenograft studies.

Conclusions and Implications: AB521 is a potent, selective and orally bioavailable HIF-2α inhibitor, with favourable pharmacological properties, that is being explored clinically for the treatment of ccRCC.

Abbreviations: ARNT, aryl hydrocarbon receptor nuclear translocator; ccRCC, clear cell renal cell carcinoma; 2-D, two dimensional; FDA, U.S. Food & Drug Administration; HIF, hypoxia-inducible factor; HUVEC, human umbilical vein endothelial cells; IHC, immunohistochemistry; PBMC, peripheral blood mononuclear cell; PD, pharmacodynamics; PK, pharmacokinetics; PO, given orally; QD, once daily; TAM, tumour associated macrophage; TKI, tyrosine kinase inhibitor; TME, tumour microenvironment; Zim, zimberelimab.

KEYWORDS
AB521, casdatifan, clear cell renal cell carcinoma, HIF-2α, renal cancer, small molecule inhibitor, VHL mutation

1 | INTRODUCTION

Hypoxia-inducible factors (**HIFs**) are transcription factors that facilitate physiological adaptations and survival in low oxygen (hypoxic) conditions. However, when expressed by cancer cells or cells in the tumour microenvironment (TME), HIFs can drive tumour growth and progression through the activation of protumourigenic transcriptional networks (Yuan et al., 2024). HIFs consist of an oxygen-regulated α monomer (**HIF-2α** being the focus of this work) that dimerizes to a constitutively expressed β monomer (HIF-1β; also known as ARNT) to become transcriptionally active. When oxygen is abundant (normoxic conditions), **proline** residues in HIF-2α are hydroxylated by prolyl hydroxylase domain (PHD) enzymes using O_2 as a substrate. Hydroxylated prolines enable recognition of HIF-2α by the von Hippel–Lindau protein (**pVHL** (Alexander, Fabbro, et al., 2023)) and subsequent ubiquitination by the pVHL-associated E3-ubiquitin ligase complex, thus marking HIF-2α for degradation by the proteosome (Ortmann, 2024; Yuan et al., 2024). In hypoxic conditions, hydroxylation cannot occur, and the canonical degradation pathway is halted. Newly stabilized HIF-2α translocates to the nucleus to bind to ARNT and activates target gene transcription. Genetic and epigenetic alterations also can drive molecular changes that mimic hypoxia, causing HIF-2α to be stabilized and transcriptionally active even when oxygen is abundant. This 'pseudohypoxic' state is commonly driven by a lack of pVHL, as is the case with inactivating *VHL* mutations, or an accumulation of citric acid cycle intermediates that inhibit PHD enzymes (Ortmann, 2024; Yuan et al., 2024).

HIF-2α-driven responses to hypoxia or pseudohypoxia can be hijacked by cancer cells and cells of the tumour microenvironment to activate protumourigenic pathways that foster angiogenesis, cell proliferation, metastasis, and survival (Davis et al., 2022; Ortmann, 2024; Yuan et al., 2024). Preclinical studies support potential protumourigenic roles for HIF-2α in renal (Chen et al., 2016; Cho et al., 2016; Kondo et al., 2003), hepatic (Foglia et al., 2022), colorectal (Ma et al., 2017; Shay et al., 2014; Xue et al., 2012; Xue et al., 2016), breast (Fu et al., 2019; Guillen-Quispe et al., 2023; Yan et al., 2022), and pancreatic cancers (Criscimanna et al., 2013; Garcia Garcia et al., 2022; Jonasch et al., 2021; Schofield et al., 2018). Additionally, HIF-2α was shown to promote angiogenic pathways in endothelial cells (Skuli et al., 2009; Skuli et al., 2012), migration and polarization of macrophages (Imtiyaz et al., 2010; Takeda et al., 2010), and mobilization of tumour associated macrophages (TAMs) by cancer-associated fibroblasts (Garcia Garcia et al., 2022).

Although HIF-2α was originally considered undruggable, the discovery of a hydrophobic pocket in the PAS-B domain of HIF-2α enabled development of small molecule allosteric inhibitors that interfere with HIF-2α/ARNT heterodimerisation, thus blocking HIF-2α-mediated transcription (Toledo et al., 2023). Clinically, HIF-2α inhibition has shown compelling safety and efficacy results (Choueiri et al., 2021; Courtney et al., 2017; Courtney et al., 2020; Jonasch et al., 2021; Jonasch, Bauer, et al., 2024), leading to the U.S. Food & Drug Administration (FDA) approval of the HIF-2α inhibitor **MK-6482** (PT2977, belzutifan) for the treatment of *VHL* disease-associated cancers (Fallah et al., 2022), advanced ccRCC (U.S. Food & Drug Administration, 2023) where inactivating *VHL* mutations are prevalent (Büscheck et al., 2020; Young et al., 2009), and most recently pheochromocytoma or paraganglioma (FDA, 2025). Validation of HIF-2α as a tractable drug target has prompted additional investigations into combinatorial therapeutic approaches in various indications and development of next-generation HIF-2α inhibitors (Nguyen et al., 2024). Here, we characterize the pharmacology of a novel small molecule inhibitor of HIF-2α, AB521 (casdatifan) (Hardman et al., 2025; Mata et al., 2025), which was discovered using a pharmacophore mapping and structure-based design approach. AB521 potently and selectively inhibits HIF-2α-mediated transcription, is orally bioavailable with favourable pharmacokinetic properties, and demonstrates effective antitumour activity in ccRCC xenograft models both as a single agent and in combination with other clinically relevant therapeutics.

What is already known

- HIF-2α promotes tumour progression in settings such as *VHL*-mutant ccRCC.
- HIF-2α inhibition is an FDA-approved treatment strategy for select oncology indications.

What does this study add

- Pharmacological evaluation of AB521 shows it is a potent and orally bioavailable HIF-2α inhibitor.
- Inhibition of HIF-2α by AB521 disrupts protumourigenic gene transcription in cancer, stromal, and immune cells.

What is the clinical significance

- AB521 is undergoing evaluation in clinical trials as a treatment for cancer.
- Improved tumour control occurs by combining AB521 with a tyrosine kinase inhibitor or anti-PD-1 antibody.

2 | MATERIALS AND METHODS

2.1 | Materials

AB521 (casdatifan) (Hardman et al., 2025; Mata et al., 2025), MK-6482/PT2977 (belzutifan) (Xu et al., 2019), and **PT2385** (Wehn et al., 2018) were synthesized by Arcus Biosciences and dissolved in 100% DMSO prior to in vitro use and formulated for in vivo studies as indicated under the mouse xenograft models subsection. For mouse in vivo studies, purified human anti-**PD-1** antibody (**zimberelimab**, zim) (Lou et al., 2021; Markham, 2021) was supplied by Arcus Biosciences, whereas purified human IgG4 isotype control antibody (CrownVivo human IgG4, MBL International) and **cabozantinib** (MedChemExpress) were sourced commercially.

2.2 | Cell lines

HEK293T (ATCC CRL-3216, RRID:CVCL_0063), A-498 (ATCC HTB-44, RRID:CVCL_1056), Hep3B (ATCC HB-8064, RRID:CVCL_0326), and 786-O (ATCC CRL-1932, RRID:CVCL_1051) cell lines were obtained from the American Type Culture Collection (ATCC) and cultured in EMEM (A-498), DMEM (Hep3B, HEK293T), or RPMI-1640 (786-O) media supplemented with 10% FBS, 100 $U \cdot ml^{-1}$ penicillin/streptomycin, and 1× GlutaMAX (all Gibco). Human Umbilical Vein Endothelial Cells (HUVECs) were obtained from ATCC and cultured in EBM-2™ media (Lonza) with EGM-2 BulletKit™ Supplement (Lonza). Cell lines were authenticated using short tandem repeat DNA profiling and tested for pathogen contamination including *Mycoplasma* spp. (STAT-Myco and IMPACT II testing) via qPCR (IDEXX Bioresearch). All cell lines were maintained at 37°C, 21% O_2, 5% CO_2. For hypoxic culture conditions, cells were incubated in a hypoxia incubator (Thermo Scientific Heracell™ VIOS 160i) set at 1% O_2, 37°C, 5% CO_2.

2.3 | Co-immunoprecipitation

Gene sequences of full-length HIF-2α (aa 1–870) with a C-terminal Flag tag and ARNT (aa 1–789) with a C-terminal Myc tag were synthesized in recombinant expression plasmid pCDNA3.1 by Genscript and used for co-immunoprecipitation. Co-immunoprecipitation of HIF-2α with ARNT was performed using similar protocols as reported previously (Wu et al., 2019). HEK293T cells grown in DMEM containing 10% FBS and 1× GlutaMAX (Gibco) were seeded in 150-mm dishes and incubated at 37°C with 5% CO_2. After 24 h, cells were transfected with 3 μg of HIF-2α and 6 μg of ARNT plasmids using jetPRIME reagent (Polyplus) following manufacturer's protocol. After overnight incubation, medium was replaced with media containing AB521 or MK-6482 in 0.25% DMSO. The following day, cells were harvested and sonicated in Lysis Buffer (50-mM Tris pH 7.5, 150-mM NaCl, 1-mM EDTA, 1%Triton X-100, 1× Roche cOmplete Protease Inhibitor Cocktail). Lysates were clarified by centrifugation at 5000× gravity for 20 min. Supernatants were quantified by BCA. Immunoprecipitation of 1-mg clarified lysate was performed with 50 μl of ANTI-FLAG M2 affinity gel (Sigma A2220, RRID:AB_10063035) following the manufacturer's protocol. Proteins were visualized by immunoblotting using an anti-FLAG antibody (Sigma F1804, RRID:AB_262044) and anti-Myc antibody (CST 2278, RRID:AB_490778). Image capture was performed using an LI-COR Odyssey. Quantification of blots was performed using LI-COR Image Studio software.

2.4 | 786-O VEGF secretion assay

786-O cells were plated at 1×10^4 cells per well and treated either with vehicle (1% DMSO), AB521, or MK-6482 at indicated concentrations overnight. The following day, media was replaced with fresh media containing DMSO or compound for an additional 24 h incubation. VEGF secretion in the cell supernatant was quantified using VEGF AlphaLISA™ (Perkin-Elmer). Data were normalised to 100% activity with DMSO treated cells with 0% activity set to a within-run standard based on cells treated with 1 μM PT2385.

2.5 | Immunoblots

For in vitro studies, 1×10^6–4×10^6 cells were cultured as indicated and protein was harvested in 100–200 μl of RIPA buffer (Abcam) containing phosphatase inhibitors 2 and 3 (Sigma-Aldrich), and cOmplete™ protease inhibitor cocktail (Roche). For excised xenograft tumours, flash frozen tumour samples were stored in Omni ceramic bead tubes (Revvity) and homogenized in 500 μl of RIPA buffer with phosphatase and protease inhibitors using an Omni International Bead Ruptor Elite bead mill homogenizer. Lysates were sonicated and then cleared of debris by centrifugation at 5000× gravity for 10 min at 4°C. Protein was denatured using NuPAGE LDS sample buffer (Invitrogen) according to the manufacturer's instructions and samples were run on a 4%–12% Bis-Tris gel (Invitrogen). Gel transfer to nitrocellulose was performed using an iBlot™ 2 dry transfer system (ThermoFisher) with iBlot™ 2 nitrocellulose transfer stacks (LifeTechnologies, 0.2 μm pore size, 100% pure nitrocellulose, protein binding capacity of 209 $\mu g \cdot cm^{-2}$ protein-binding capacity). Nitrocellulose blots were blocked with 5% milk in TBS-T, washed 3× with TBS-T, then incubated with primary antibodies diluted in 5% milk in TBS-T: rabbit antihuman HIF-2α (clone D9E3, RRID:AB_10898028 or clone D6T8V, RRID:AB_2799579, Cell Signaling Technology, or Abcam clone BL-95-1A2, RRID:AB_2631884, all used at 1:1000), rabbit antihuman HIF-1α (clone EPR16897, RRID:AB_2941086, Abcam, used at 1:1000), rabbit anti-ARNT (clone D28F3, RRID:AB_2783880, Cell Signaling Technology, used at 1:1000) or mouse antihuman/mouse β-actin (clone 8H10D10, RRID:AB_2242334, Cell Signaling Technology, used at 1:2000). Blots were washed again with TBS-T and incubated with goat anti-rabbit HRP (#PI-1000, RRID:AB_2336198, Vector Labs, used at 1:10,000) and goat anti-mouse 800CW (#NC0824545, RRID:AB_2687825, Li-COR, used at 1:10,000) in 5% milk in TBS-T. Blots were washed once more in

TBS-T and then visualized using SuperSignal™ West Atto Ultimate Sensitivity Substrate (Thermo Fisher) on a LI-COR Odyssey. Quantification was done using Image Studio™ Lite software.

2.6 | ARNT siRNA and CRISPR/Cas9

For siRNA experiments, 786-0 or A-498 cell lines were rested overnight in appropriate antibiotic-free media, as indicated previously, before transfecting with 0.5 μM of nontargeting control or ARNT-specific siRNA pools, with each pool comprised of four distinct siRNAs (specified below) using DharmaFECT reagent (Dharmacon) following the manufacturer's standard transfection protocol. Transfected cells were incubated at 37°C for 48 h in antibiotic-free media and then another 24 h in media with antibiotics before collecting for immunoblot analysis. Control siRNA (ON-TARGET plus Non-targeting Pool) and ARNT-specific siRNA (ON-TARGET plus Human ARNT siRNA SMARTpool) were purchased from Dharmacon. Non-targeting siRNA sequences were as follows: siRNA-1: UGGUUUACAUGUCGACUAA; siRNA-2: UGGUUUACAUGUUGUGUGA; siRNA-3: UGGUUUACAUGUUUUCUGA; siRNA-4: UGGUUUACAUGUUUUCCUA. ARNT-targeting siRNA sequences were as follows: ARNT-siRNA-1: UCAGAUGUCUAACGAUAAG, ARNT-siRNA-2: GGACUUGGCUCUGUAAAGG; ARNT-siRNA-3: CCACUGAUGGCUCCUAUAA; ARNT-siRNA-4: GUAGUGCCCUGGCUCGAAA. For CRISPR/Cas9-mediated ARNT knockout experiments, multiple gRNAs were designed targeting Exon 6 of the ARNT gene (sequences listed below). One day before nucleofection, lyophilized gRNAs were dissolved in TE buffer to a final concentration of 50 μM. On the day of nucleofection, Cas9 protein (#1081060, IDT) was diluted to a final concentration of 6.2 μM in Lonza SF nucleofection buffer (#V4XC-9064, Lonza). All three gRNAs were combined, and Cas9 protein was added and gently mixed, resulting in an approximate 1:5 ratio of Cas9 protein to gRNA. 2×10^5 cells were added to the ribonucleoprotein complex after 15 min of incubation at room temperature. 786-O cells were nucleofected using condition DN-100 and A-498 were nucleofected using condition DS-138 by the Lonza 4D nucleofection system. Sanger sequencing was performed to validate knockout efficiency by Synthego's ICE Analysis tool 3 days post-nucleofection (Conant et al., 2022). ARNT guide RNA sequences were as follows: guide-1: ACTGGCAACACATCCACTGA; guide-2: TCTCACATGAAGTCCTTGCG; guide-3: CAAGCTAACCATCTTACGCA.

2.7 | Cell growth and viability assays

Cell growth and viability were measured using either CellTiter-Glo® 2.0 according to the manufacturer's instructions, or by flow cytometry-based analysis where indicated. For flow cytometry analysis, cells were trypsinized, washed in PBS, and then resuspended in 1× BD Pharmingen™ Annexin V Binding Buffer (#556454, BD Biosciences) containing cell permeable viability dye (1:1000, LIVE/DEAD™ Fixable Near-IR Dead Cell Stain Kit, Invitrogen) and Annexin V stain (1:20, RRID:AB_2869071, BD Biosciences) and incubated for 15 min at room temperature protected from light. Cells were then pelleted by centrifugation (400× gravity for 10 min at 4°C), washed with 1× Annexin V Binding Buffer, and then fixed (eBiosciences™ IC Fixation Buffer). Flow cytometry was performed using an LSRFortessa™ X-20 cytometer (BD Biosciences) with subsequent analysis conducted using FlowJo™ analysis software.

2.8 | 786-O anchorage-independent growth assay

In 12-well culture plates, 786-O cells were suspended at 2.5×10^3 cell per well in 1× supplemented RPMI-1640 with 0.4% agarose, layered above a 1× supplemented RPMI-1640 with 1% agarose base layer. A 400 μl per well feeder layer of supplemented RPMI-1640 was added on top of each well followed by the addition of either DMSO, AB521, or MK-6482 at indicated concentrations using a D300 digital dispenser (Hewlett-Packard) with a final DMSO concentration of 0.1%. Cultures were maintained at 37°C, 5% CO_2, and medium containing 0.1% DMSO or compound was carefully replaced every 3–4 days. After 21 days, the medium layer was removed, colonies were stained using 250 μl per well of a 0.005% crystal violet solution (Sigma-Aldrich) and incubated for 1 h at room temperature. After washing thoroughly with water, colonies were quantified using an inverted microscope. Four 5× magnification fields were analysed for each well to determine the average number of colonies per field per well. Five independent experiments, each containing three to four biological replicates, were performed. For each independent experiment, colony counts were normalised to the mean vehicle (0.1% DMSO) colony count of that respective experimental iteration.

2.9 | Hep3B and HUVEC gene expression assay

Hep3B or HUVECs were plated at 1×10^5 cells·ml^{-1} per well in 24- or 12-well culture plates and incubated at 37°C, 5% CO_2 at 21% O_2 for 6–8 h. Media was replaced with 1 ml per well of fresh media containing either DMSO or AB521 at indicated concentrations with a final DMSO concentration of 0.1%. Cells were incubated at 37°C, 5% CO_2 in either 21% or 1% O_2 for 20 h and then collected for RNA extraction and RT-qPCR; see RT-qPCR subsection for procedure details.

2.10 | Primary human M2-polarised macrophage assay

Peripheral blood mononuclear cells (PBMCs) were isolated from healthy donor leukocyte reduction system chambers obtained from the Stanford Blood Center with informed written consent and according to IRB-approved human sample guidelines in accordance with U.S. Common Rule. **CD14**$^+$ monocytes were isolated using the EasySep™ Human CD14 Positive Selection Kit (StemCell

Technologies). Monocyte-derived M0 macrophages were generated by resuspending $CD14^+$ monocytes in 6-well cell culture plates in RPMI-1640 supplemented with 10% FBS and recombinant human M-CSF (50 ng·ml^{-1}, R&D Systems) for 6 days. On day 6, 100 µl per well of IL-4 (final concentration 20 ng·ml^{-1}, Peprotech) was added to each well along with either DMSO or 1 µM AB521 with a final DMSO concentration of 0.1%. Cells were incubated at 37°C, 5% CO_2 in either 21% or 1% O_2 for 20 h and then collected for RNA extraction and RT-qPCR.

2.11 | T-cell activation assay

Isolated human T-cells were thawed and rested overnight in RPMI supplemented with 200 U·ml^{-1} IL-2 (Peprotech), 10% FBS (Gibco), 1× GlutaMAX (Gibco) and 100 U·ml^{-1} penicillin/streptomycin (Gibco). The cells were then labelled with the proliferation tracking dye (CellTrace™ Violet, Thermo) by incubating 1×10^6 cells·ml^{-1} resuspended in HBSS with 5 nM of reconstituted dye for 20 min at 37°C with 5% CO_2, avoiding exposure to light. Next, five volumes of cold HBSS + 2% FBS were added to the cells and incubated for 5 min. Cells were washed 3× with HBSS + 2% FBS at 300× gravity for 10 min. Cells were resuspended in CTS Optimizer medium (Gibco) and activated using a T-cell activation/expansion kit (Miltenyi Biotec) with bead-bound anti-CD2, anti-CD3, and anti-CD28 according to the manufacturer's instructions with a 1:1 bead:cell ratio. After addition of activation beads and/or HIF-2α inhibitor compounds, cells were cultured for 1 h at 37°C 21% O_2, then moved to a hypoxic chamber (37°C, 1% O_2) and cultured for 3 days. The degree of cell proliferation was then assessed in $CD8^+$ T-cells by flow cytometry based on changes in CellTrace™ Violet staining, whereas secretion of IFNγ into the cell supernatant was determined by cytometric bead array (BD Biosciences).

2.12 | RT-qPCR

RNA was isolated using the RNeasy Mini Kit (Qiagen) and converted to cDNA using Superscript IV First Strand Synthesis (Invitrogen) according to the manufacturer's instructions. RT-qPCR was carried out using Taqman® probes (Thermo Fisher) and a QuantStudio™ 7 Pro Real-Time qPCR machine (Applied Biosystems). Relative gene expression was calculated using the formula $2^{-\Delta Ct}$ where ΔCt equals the cycle threshold (Ct) for the gene of interest minus the Ct for the reference gene. Probe information is listed in Table S1.

2.13 | Mice

Female 6- to 8-week-old NU-*Foxn1*^{nu} (Strain #088) mice were purchased from Charles River Laboratories. Female 4- to 5-week-old NSG-MHC I/II DKO (Strain #025216) mice were purchased from Jackson Laboratories. Experiments were performed at Arcus Biosciences in accordance with federal, state, and institutional guidelines and were approved by Arcus Biosciences' Institutional Animal Care and Use Committee. Animal studies are reported in compliance with the ARRIVE guidelines (Percie et al., 2020) and with the recommendations made by the British Journal of Pharmacology (Lilley et al., 2020).

2.14 | Mouse xenograft models

Athymic nude mice were anaesthetized by exposure to 3–4% isoflurane (Piramal Critical Care) delivered via a vaporizer (Vetequip) in an enclosure for 5 min and then injected subcutaneously (s.c.) on the right flank with 4×10^6 786-O or A-498 cells in 100 µl of 1:1 solution of PBS:Matrigel (Corning). For single agent efficacy, mice were randomised based on an average tumour volume of ~200 mm^3 (786-O) or ~250 mm^3 (A-498) and treated with vehicle (PEG400:Kolliphor HS15 70:30) or AB521 orally (PO) once-daily (QD). For combination efficacy of AB521 with cabozantinib, mice were randomised based on an average tumour volume of ~550 mm^3 and treated with saline, cabozantinib, vehicle, or AB521 PO QD. For studies using PT2385, the compound was formulated in 10% EtOH, 30% PEG400, 60% MCT (0.5% methylcellulose, 0.5% Tween 80). For all xenograft studies, tumour volume was monitored with digital callipers and calculated using the formula: (length × width^2)/2. Experiments were not blinded because the same operators performed drug delivery and collected tumour measurements.

2.15 | Humanized peripheral blood mononuclear cell (PBMC) A-498 ccRCC xenograft mouse model

Female NSG-MHC I/II DKO mice were anaesthetized by exposure to 3–4% isoflurane (Piramal Critical Care) delivered via a vaporizer (Vetequip) in an enclosure for 5 min and then inoculated s.c. on the right flank with 4×10^6 A-498 cells in 100 µl of 1:1 ratio of PBS:Matrigel. Once tumours were established, mice were again anaesthetized as before and injected intravenously with 2×10^7 human PBMCs. Seven days later, blood was collected to check the engraftment of human CD45-positive cells. Mice were randomised based on human $CD45^+$ engraftment and tumour volume prior to treatment. Vehicle or 30 mg·kg^{-1} AB521 were given orally (PO) once-daily (QD), whereas 10 mg·kg^{-1} of human IgG4 isotype or human anti-PD-1 antibody (zimberelimab, zim), both in HBSS, were given interperitoneally (i.p.) every 3 days (Q3D) to the indicated cohorts. Donor PBMC and tumour cell HLA matching was not performed.

2.16 | Pharmacokinetic (PK) and pharmacodynamic (PD) assessments in mice

For PK assessment, plasma was collected at 0, 2, 6, 10, 18, and 24 h after a single PO dose of drug and drug levels were measured by

liquid chromatography-mass spectrometry (LC–MS). For PD assessment, 786-O, or A-498 tumours were collected and snap-frozen 24 h either after vehicle or AB521 PO dosing. RNA was extracted and RT-qPCR was performed. For measurement of VEGF protein, plasma was isolated from the blood of 786-O or A-498 tumour-bearing mice 12 h after the last dose of vehicle or AB521 (mice were dosed PO twice daily [BID] for 10 days). VEGF protein levels were measured by cytometric bead array using human VEGF Flex set (BD Biosciences). For measurement of mouse **erythropoietin** (EPO) protein, plasma was isolated from blood of C57BL/6 mice 8 h after a single PO dose of vehicle or AB521. EPO protein levels in the plasma were measured by ELISA (mouse EPO ELISA, R&D).

2.17 | Immunohistochemistry (IHC)

Formalin fixed and paraffin embedded tissues were processed and sectioned at 4 μm thickness using standard histological procedures. Staining of the slices was carried out using a Leica BOND RX Autostainer (Leica Biosystems). Briefly, slices were dewaxed and rehydrated on the autostainer using BOND Dewax Solution, 100% Alcohol, and BOND Wash Solution (Leica Biosystems). Antigen retrieval was performed either using low pH (ER1) or high pH (ER2) buffer at 95°C for 20 min depending on the primary antibody (see Table S2 for antibody details and buffer conditions). Slices were stained using components that are part of the Leica Bond Polymer Refine Detection System (#DS9800) using default IHC protocol (Protocol F) with primary antibody incubation adjusted to 30 min. Stained slices were rinsed with distilled water and later dehydrated, and coverslipped using the DAKO coverstainer (Agilent Technologies). Slides were scanned using a 3DHistech Panoramic MIDI II Scanner (3DHISTECH), and images were analysed using HALO image analysis software (Indica Labs).

2.18 | Data and statistical analysis

The methods and analysis performed comply with *British Journal of Pharmacology* recommendations and requirements on experimental design and analysis (Curtis et al., 2018; Curtis et al., 2022). Where immunoblotting or IHC was conducted, the experimental detail provided conforms with *British Journal of Pharmacology* guidelines (Alexander et al., 2018). Studies were designed to generate groups of equal size, where group size represents independent values (donors, animals, or independent repeats). Statistical analyses were completed using Prism (GraphPad) or R. Statistical analysis was undertaken only for studies where each group size was at least $n = 5$. Experiments with $n < 5$ were included in some instances and are marked accordingly as qualitative comparisons. IC_{50} values were calculated using a nonlinear four-parameter fit of $\log_{10}$ transformed data. In multigroup studies with parametric variables, post hoc tests were conducted only if F in ANOVA (or equivalent) achieved the necessary level of statistical significance and no significant difference in homogeneity was observed, or for instances where homogeneity differed between groups a Brown–Forsythe and Welch's ANOVA was performed. For repeat measures, ANOVA sphericity was not assumed and a Geisser–Greenhouse correction was applied. Outliers were included in all data analysis and presentation. Data normalisation was performed on the VEGF secretion assay and anchorage-independent growth assay, as noted elsewhere in the Methods section, as a way of anchoring the data to a commonly run reference or control to adjust for cross-experiment differences in output, with Y axis labelled accordingly as the percent of the control value. For all statistical tests, P values <0.05 were considered significant.

2.19 | Nomenclature of targets and ligands

Key protein targets and ligands in this article are hyperlinked to corresponding entries in https://www.guidetopharmacology.org and are permanently archived in the Concise Guide to PHARMACOLOGY 2021/22 (Alexander et al., 2021; Alexander, Kelly, et al., 2023).

3 | RESULTS

3.1 | AB521 potently and selectively inhibits HIF-2α-dependent transcription

A pharmacophore mapping and structure-based design approach was used to create the novel small-molecule HIF-2α inhibitor, AB521, also known as casdatifan (Hardman et al., 2025; Mata et al., 2025) (Figure 1a). AB521 was designed to bind the PAS-B domain of HIF-2α, effectively inhibiting HIF-2α-ARNT complex formation and HIF-2α-mediated transcription. Disruption of HIF-2α-ARNT dimerisation by AB521 was confirmed by co-immunoprecipitation using an overexpression system in which Flag-tagged HIF-2α and Myc-tagged ARNT were co-transfected into HEK293T cells. The amount of ARNT protein immunoprecipitated with HIF-2α was reduced in a concentration-dependent manner when the cells were treated with AB521 or MK-6482 (belzutifan, PT2977) (Choueiri et al., 2024; Xu et al., 2019) (Figure 1b). Further characterization of AB521 was performed using the 786-O ccRCC cell line, which does not express functional pVHL or HIF-1α (Shinojima et al., 2007), and for which HIF-2α is known to be a cell-intrinsic driver of 786-O xenograft growth (Kondo et al., 2003). Because 786-O cells lack functional pVHL, and therefore exist in a pseudohypoxic state, activity of AB521 was assessed in normal oxygen conditions (21% O_2). Treatment of 786-O cells with AB521 or MK-6482 caused a marked reduction in HIF-2α protein (Figure 1c), a finding that has been reported with other HIF-2α inhibitors (Cho et al., 2016; Yan et al., 2022). Notably, the reduction in HIF-2α caused by either AB521 or MK-6482 cannot be directly attributed to disruption of HIF-2α-ARNT heterodimerisation, because HIF-2α expression was not reduced when ARNT was made unavailable by depletion using siRNA or CRISPR/Cas9 approaches (Figure S1). Taken together, these data show that AB521 can block HIF-2α-ARNT

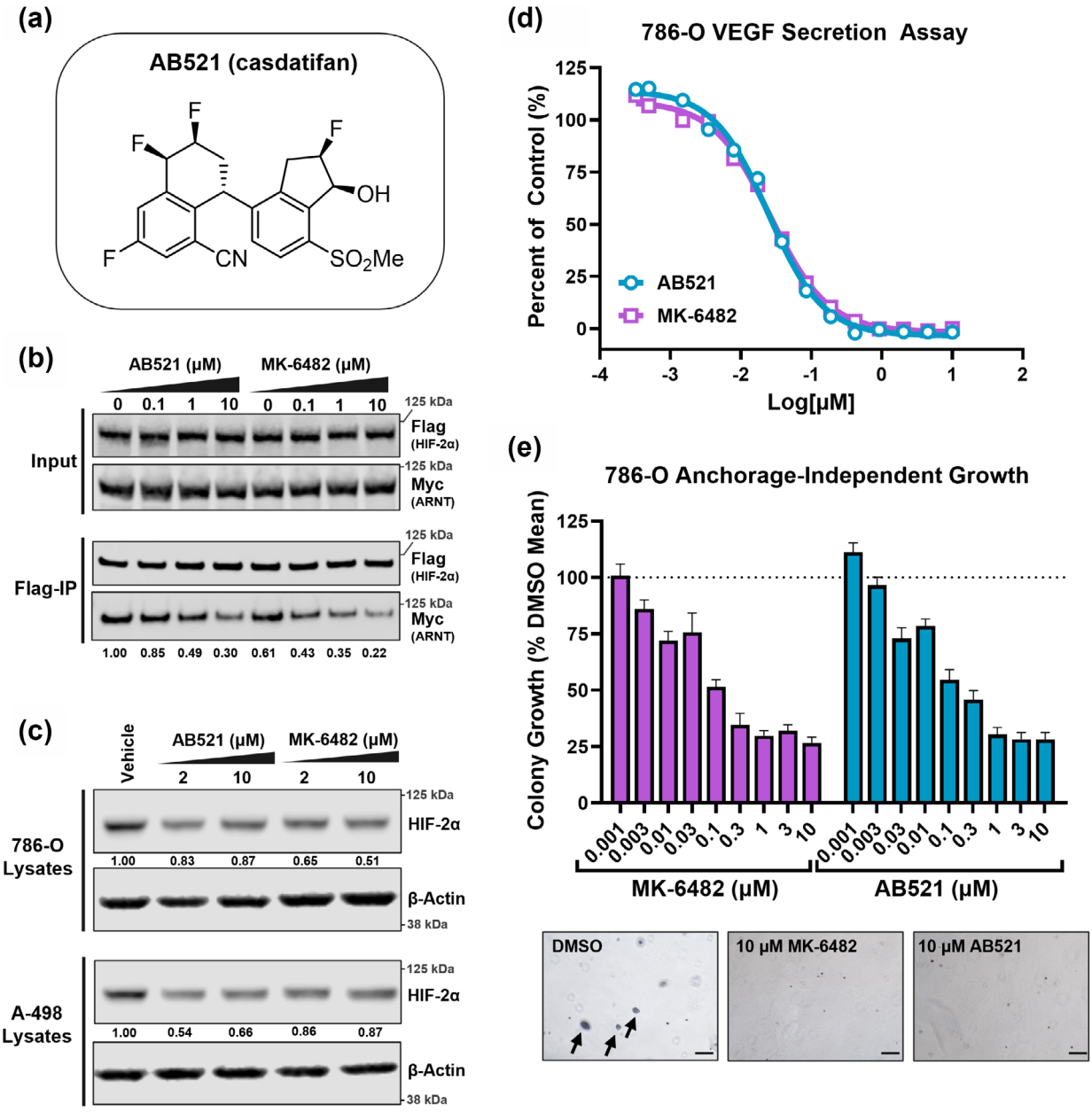

FIGURE 1 AB521 inhibits HIF-2α-dependent transcription and anchorage-independent growth in *HIF1A* and *VHL* mutated 786-O ccRCC cells. (a) The chemical structure of AB521 (casdatifan). (b) Immunoblots from HEK293T cells transfected with Flag-tagged HIF-2α and Myc-tagged ARNT. Anti-Flag (HIF-2α) immunoprecipitates (Flag-IP) and whole-cell extracts (Input) blotted for Flag (HIF-2α) and Myc (ARNT) are shown. Quantification of the HIF-2α/ARNT signal ratio from the Flag-IP blot relative to the first vehicle control is shown below the lowest blot image. (c) Immunoblots showing HIF-2α protein expression from 786-O or A-498 cell lysates following overnight treatment with either AB521 or MK-6482 at 2 μM or 10 μM. Quantification of the HIF-2α/β-actin ratio normalised to the vehicle control group is provided between blot images. (d) Endogenously expressed and secreted VEGF was measured in media from 786-O cell cultures after incubation with either AB521 or MK-6482 for 24 h. Results show representative data from a single experiment presented relative to controls. AB521 ($n = 11$, $IC_{50} = 28.9 \pm 3.6$ nM), MK-6482 ($n = 13$, $IC_{50} = 31.6 \pm 19.4$). (e) Anchorage independent colony formation of 786-O cells was quantified following a 21 day culture period. Graph shows mean ± standard deviation (SD) of data from $n = 5$ independent experiments with $n = 3$–4 biological replicates per experiment. Colony counts from each independent experiment were normalised to the mean vehicle (0.1% DMSO) count from that experimental iteration, and results are shown as percent of the DMSO control group (dotted line). Example images of 786-O colony growth in the vehicle (0.1% DMSO), 10 μM AB521, and MK-6482 treated samples are shown. Arrows indicate multi-cellular colonies, scale bar = 200 μm.

complex formation and reduce HIF-2α protein, although the mechanism of this latter observation has not been fully elucidated.

VEGF transcription is regulated by HIF-2α in 786-O cells (Cho et al., 2016; Sowter et al., 2003; Wallace et al., 2016) and was therefore used to evaluate in vitro potency of AB521. AB521 inhibited VEGF secretion with an IC_{50} value of 28.9 ± 3.6 nM, with MK-6482 displaying an IC_{50} value of 31.6 ± 19.4 nM (Figure 1d). Although turnover rates vary by protein, these data illustrate that HIF-2α

inhibition can have acute effects on HIF-2α-regulated gene expression at the protein level. To evaluate the functional impact of AB521 on ccRCC growth in vitro, 786-O cells were cultured with either AB521 or MK-6482. Neither compound altered 786-O cell growth in standard 2-dimensional (2-D) culture, even when used at concentrations up to 10 μM (Figure S2), in agreement with previous findings examining HIF-2α inhibition on cell growth in 2-D cultures (Cho et al., 2016; Kondo et al., 2003; Wallace et al., 2016; Zimmer et al., 2004). However, several studies indicate that HIF-2α can promote anchorage independent, or 3-D spheroid, growth of cancer cells (Cho et al., 2016; Cimmino et al., 2016; Hallis et al., 2023; He et al., 2019; Hoefflin et al., 2021; Kitajima et al., 2018; Lachance et al., 2014; Stransky et al., 2022), a property often attributed to tumour initiating cells or tumour stem cells (Qureshi-Baig et al., 2017). Indeed, AB521 inhibited 786-O anchorage independent growth in a soft agar colony formation assay (Figure 1e).

The selectivity of AB521 against the other predominant HIF-α transcription factor, HIF-1α, was evaluated in Hep3B hepatocellular carcinoma (HCC) cells. In addition to expressing both HIF-1α and HIF-2α, Hep3B cells also express pVHL and therefore stabilisation of HIF-α proteins only occurs in hypoxic conditions (Figure 2a). As with 786-O and A-498 cells, treatment of Hep3B cells with AB521 led to a reduction in HIF-2α protein, whereas HIF-1α was modestly increased (Figure 2a). When exposed to hypoxia (1% O_2), Hep3B cells up-regulated HIF-1α-dependent (***PDK1*** and *PGK1*) and HIF-2α-dependent (*EPO* and *SERPINE1*) target genes (Geis et al., 2015; Kim et al., 2006; Lu et al., 2011; Rankin et al., 2007; Wallace et al., 2016) (Figure 2b,c). Overnight treatment of hypoxic Hep3B cells with AB521 resulted in concentration-dependent inhibition of HIF-2α-mediated transcription, based on decreased *EPO* and *SERPINE1* expression (Figure 2d), whereas HIF-1α target gene expression was unaffected (Figure 2e). No AB521-dependent changes in target gene expression were observed when Hep3B cells were cultured in normoxia (Figure S3A,B), and AB521 had no impact on Hep3B cell viability, indicative of a lack of off-target cytotoxicity (Figure 2f, S3C). Together, these data confirm that AB521 potently and selectively inhibited HIF-2α in both pseudohypoxic (*VHL*-mutated) and hypoxic (pVHL-expressing) cancer cells in vitro.

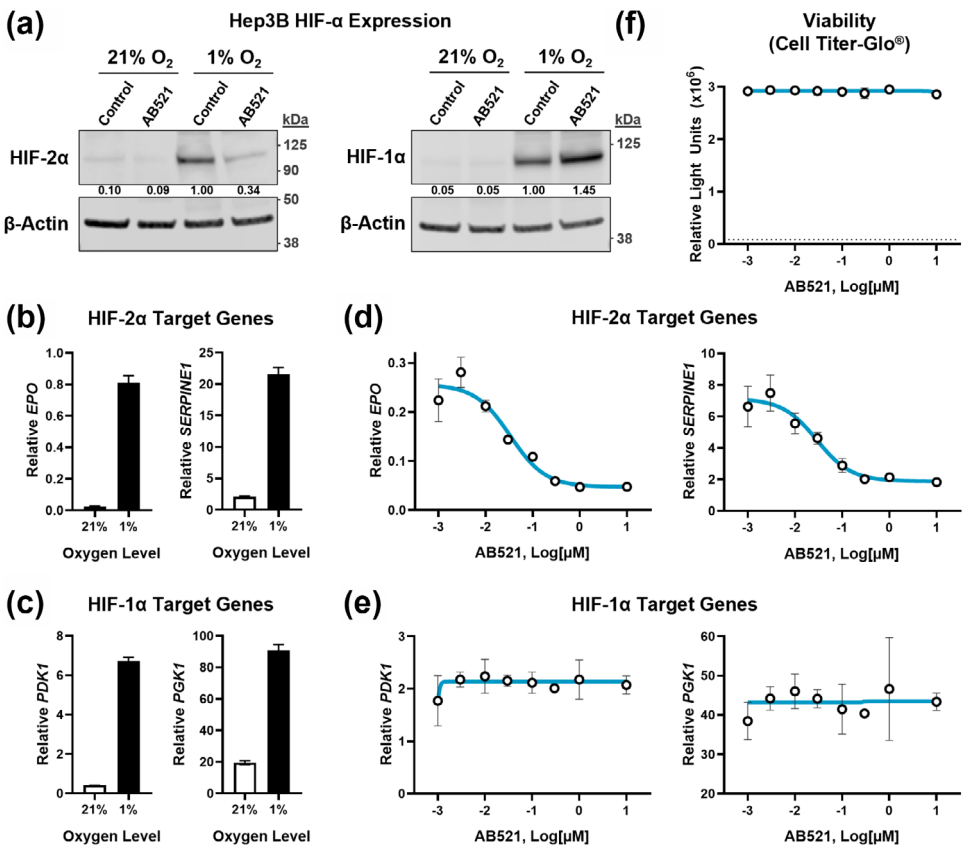

FIGURE 2 AB521 selectively inhibits HIF-2α and not HIF-1α. (a) Immunoblots showing HIF-1α and HIF-2α protein expression in Hep3B cells after overnight culture in normoxic (21% O_2) or hypoxic (1% O_2) conditions treated with 0.1% DMSO (control) or 1 μM AB521. Quantification of the HIF-α/β-actin ratio normalised to the hypoxia vehicle control group is provided between blot images. (b) HIF-2α (*EPO*, *SERPINE1*) and (c) HIF-1α (*PDK1*, *PGK1*) target gene expression in Hep3B cells after overnight culture in 21% or 1% O_2, as measured by RT-qPCR. The effect of AB521 treatment on (d) HIF-2α or (e) HIF-1α target gene expression in hypoxic (1% O_2) Hep3B cells was quantified by RT-qPCR. (f) Cell viability of AB521 treated hypoxic Hep3B cells was quantified using CellTiter-Glo®. Dotted line represents viability using a cytotoxic 20% DMSO treatment. Bars or lines and error represent the mean ± SD. Graphs show representative data from n = 5 independent experiments.

3.2 | AB521 inhibits endogenous HIF-2α-dependent gene transcription in primary human cells

Based on the reported roles for HIF-2α in primary cell types relevant to the tumour microenvironment (TME), namely, macrophages (Imtiyaz et al., 2010; Takeda et al., 2010) and endothelial cells (Skuli et al., 2009; Skuli et al., 2012), the ability of AB521 to inhibit HIF-2α-mediated gene transcription was assessed using respective in vitro model systems: $CD14^+$ monocyte-derived M2-polarised macrophages and human umbilical vein endothelial cells (HUVECs). Importantly, both cell types demonstrated hypoxia-inducible HIF-2α protein accumulation (Figure S4A,B). As an aside, although HIF-1α protein expression was hypoxia-dependent in HUVECs (Figure S4B), M2 polarised macrophages showed no distinct increase in HIF-1α protein quantity upon hypoxic culture, but rather displayed a higher molecular weight migration shift in the immunoblot (Figure S4A). The presence of detectable HIF-1α in the M2 polarised macrophages in normoxia was unexpected, but could be related to IL-4 treatment, which has been shown to cause HIF-1α stabilization in macrophages (Li et al., 2018). Additionally, the reason for the molecular weight shift of HIF-1α is unclear, but could be the result of oxygen-dependent post-translational modification to HIF-1α (Albanese et al., 2021).

Using M2 macrophages derived from 10 healthy donors, the effects of AB521 on gene transcription were evaluated. HIF-2α target genes of interest were previously identified in publicly available datasets and relevant publications (Courtney et al., 2020; Downes et al., 2018; Florczyk et al., 2011; White et al., 2004) and were confirmed internally to be HIF-2α-dependent in M2 macrophages. AB521 significantly blocked transcription of hypoxia-dependent HIF-2α-regulated genes involved in angiogenesis (***ADM***, *NDRG1*), extracellular matrix remodelling (*SERPINE1*, ***PDGFB***), and myeloid cell recruitment (***CXCL8***) (Figure 3a). Because HIF-2α functions in a cell-type specific manner (Smythies et al., 2019), HIF-2α regulated genes relevant to HUVECs, as opposed to macrophages, were identified based on a publicly available endothelial cell transcriptomics study (Downes et al., 2018) and confirmed internally. In HUVECs, AB521 significantly inhibited hypoxia-dependent increases in HIF-2α-regulated transcription of genes involved in angiogenesis (*ADM*, ***DLL4***, *AKAP12*) and glycolytic metabolism (***SLC2A1***, *SLC2A3*) (Figure 3b). Notably, preliminary analysis showed no impact of AB521 on HUVEC cell growth and viability in vitro (Figure S4C,D). Taken together, these results demonstrate the ability of AB521 to block hypoxia-driven HIF-2α-dependent gene transcription in TME-relevant cell types such as human macrophages and endothelial cells.

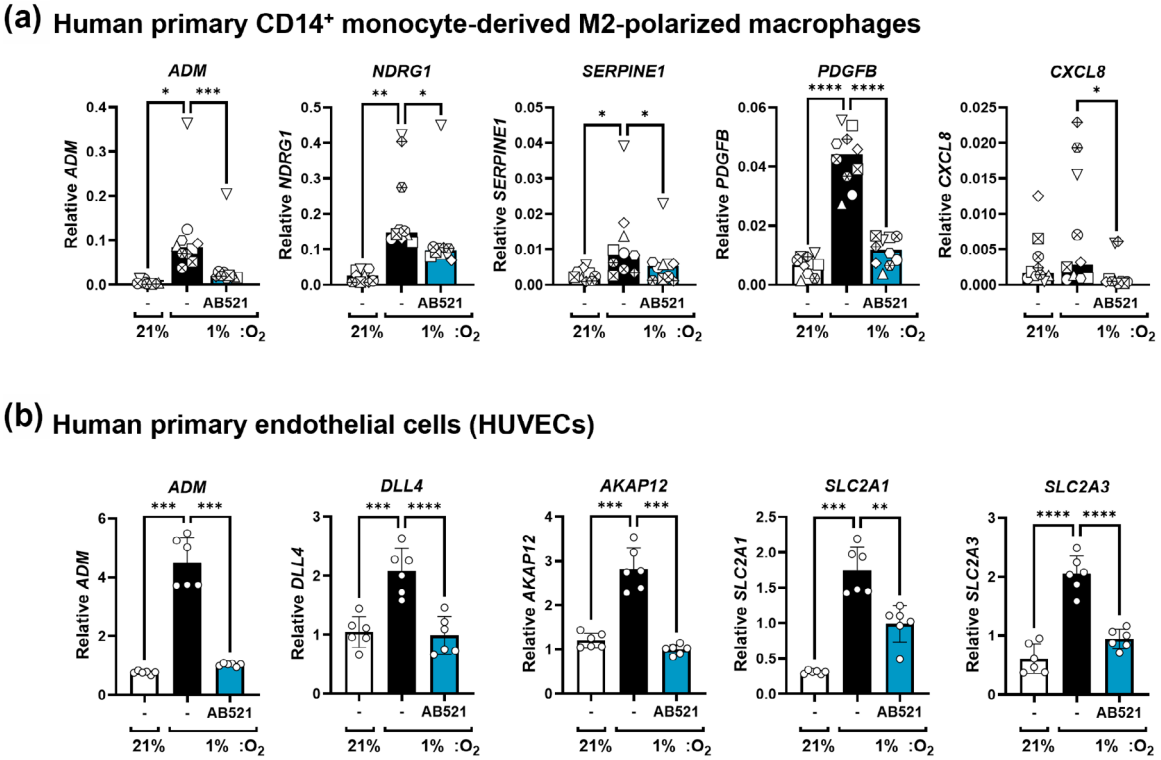

FIGURE 3 AB521 inhibits HIF-2α-dependent gene expression in primary human macrophages and endothelial cells. Cells were treated with either vehicle (0.1% DMSO) or 1 μM AB521 and incubated in normoxia (21% O_2) or hypoxia (1% O_2) for 20 h. Target gene expression was measured by RT-qPCR for (a) human $CD14^+$ monocyte-derived M2 polarised macrophages or (b) human umbilical vein endothelial cells (HUVEC). (a) Bars and error represent the median ± range. Each symbol represents a different donor; n = 10 donors total. Analysed by repeated-measures ANOVA followed by Dunnett's multiple comparisons test. (b) Bars and error represent mean ± SD with symbols showing biological replicates (n = 6) from two independent experiments. Analysed by one-way ANOVA followed by Dunnett's multiple comparisons test. *P < 0.05, **P < 0.01, ***P < 0.001, ****P < 0.0001.

3.3 | AB521 blocks HIF-2α-mediated gene transcription in vivo and inhibits tumour growth

When given to mice via oral gavage, AB521 demonstrated favourable pharmacokinetics (PK) (Figure S5), showing oral bioavailability and enabling assessment of in vivo pharmacodynamic (PD) effects and antitumour efficacy of AB521 using oral dosing once-daily (PO QD). Circulating concentrations of EPO, a HIF-2α target expressed by interstitial fibroblasts in healthy kidney tissue (Haase, 2010), were evaluated as a peripheral PD biomarker. EPO levels were significantly decreased relative to vehicle-treated mice following a single oral dose of AB521 at either 30 or 100 mg·kg^{-1} (Figure 4a).

The effects of AB521 on the expression of tumour-associated PD markers were assessed using 786-O and A-498 *VHL*-mutant ccRCC xenograft models. Tumour-bearing mice were treated with various doses of AB521 and plasma samples and tumour lysates were collected for analysis 12 h after the final AB521 dose. Circulating levels of tumour-derived human **VEGF-A** were generally lower in AB521 treated animals, although this did not reach statistical significance (Figure 4b). Analysis of HIF-2α target gene expression in tumour tissue lysates showed statistically significant and dose-dependent decreases in *VEGFA*, *CCND1*, and ***CXCR4*** expression following AB521 treatment (Figure 4c,d), signifying effective HIF-2α inhibition within the tumour tissue. Indeed, a direct correlation was observed between the reduction in HIF-2α target gene mRNA and the corresponding plasma concentrations of AB521 (Figure 4e).

Antitumour efficacy of AB521 was evaluated using 786-O and A-498 xenograft models. Both xenograft models have been previously shown, and confirmed here, to be sensitive to HIF-2α inhibition using the first-generation inhibitor PT2385 (Wallace et al., 2016) (Figure S6). Mice bearing established tumours were treated with AB521 covering a range of concentrations and tumour volume was measured over time. In both tumour models, and at all dose levels tested, AB521 significantly reduced tumour burden relative to the vehicle control groups (Figure 5).

To further investigate the intratumoural effects of AB521, 786-O and A-498 xenograft tumours were harvested after 5 days of AB521 dosing, when the impact of AB521 on tumour growth was beginning to take effect (Figure 6a,b). Similar to the effect of HIF-2α inhibition in vitro (Figures 1c and 2a), HIF-2α protein from tumour lysates was significantly decreased with AB521 treatment (Figure 6c,d), a finding also reported for PT2385 (Wallace et al., 2016). Histological evaluation by IHC revealed a significant decrease in cell proliferation based on Ki-67 staining (Figure 6e,f). The level of Ki-67 reduction appeared reflective of the degree of tumour growth inhibition, with 786-O showing a greater reduction in both tumour volume and Ki-67 staining upon AB521 treatment compared with A-498 cells. The degree of tumour vascularization was assessed by CD31 staining and showed a modest but significant decrease with AB521 treatment in A-498 tumours, but not 786-O tumours (Figure 6e,f). Finally, cleaved caspase-3 (CC3) and phosphorylated histone (γ-H2AX) were evaluated as apoptosis markers. No change in either CC3 or γ-H2AX was observed in the 786-O tumour samples (Figure 6e). The A-498 tumours showed a significant decrease in CC3 upon AB521 treatment, and a modest, but not significant, decrease in γ-H2AX (Figure 6f), although notably the frequency of CC3 positive cells was extremely low in the A-498 samples, corresponding to < 1% of the total cells analysed.

Taken together, AB521 demonstrated a clear PK-PD relationship with dose-dependent inhibition of multiple HIF-2α-mediated PD markers in both naïve and tumour bearing mice and significantly decreased tumour burden in two ccRCC xenograft models. Evaluation of tumour samples after acute dosing with AB521 showed a distinct decrease in HIF-2α protein and a significant reduction in the number of proliferating tumour cells.

3.4 | Combination of AB521 with a tyrosine kinase inhibitor (TKI) or an anti-PD-1 antibody reduces ccRCC xenograft growth

Given the myriad of factors that influence tumour growth and progression, effective therapeutic interventions often consist of treatment combinations that target multiple pathways and cell types. In frontline ccRCC, broad targeting VEGF receptor (VEGFR) TKIs, such as cabozantinib, and immune checkpoint targeting therapies, such as **nivolumab** (anti-PD-1) and **ipilimumab** (anti-CTLA-4), are the standard of care (Motzer et al., 2022). Cabozantinib suppresses angiogenesis and inhibits metastasis and tumour growth by targeting multiple tyrosine kinases, having the strongest potency for **VEGFR2** and **c-MET** (Yakes et al., 2011). AB521, to an extent, also targets angiogenic pathways (Befani & Liakos, 2018) (Figure 3), in addition to the hundreds of other HIF-2α-regulated genes associated with metabolism, survival, epithelial-mesenchymal transition, and more (Davis et al., 2022; Downes et al., 2018; Ortmann, 2024). In combination, these agents should provide a robust multifaceted antiangiogenic activity while also targeting unique, inhibitor-specific pathways critical for ccRCC tumour growth and progression. To evaluate the combinatorial effects of AB521 with cabozantinib, both inhibitors were tested using the A-498 ccRCC xenograft model. As single agents, both AB521 (100 mg·kg^{-1}) and cabozantinib (30 mg·kg^{-1}) caused tumour growth arrest, whereas vehicle-treated animals showed uncontrolled tumour growth and most did not proceed beyond the study midpoint (Figure 7a,b). When used in combination, AB521 with cabozantinib caused A-498 tumour regression and showed a statistically significant improvement in tumour growth control compared with vehicle or single agent treatment arms. Notably, while the lower dose of cabozantinib (10 mg·kg^{-1}) only moderately delayed tumour progression as a single agent, it too caused enhanced tumour regression when used in combination with AB521.

Combining HIF-2α inhibition with an immuno-oncology agent such as anti-PD-1 could also be beneficial because each treatment offers distinctive mechanisms of action: inhibition of cancer cell-intrinsic and TME-related protumourigenic pathways in the case of AB521 and enhancement of antitumour immunity in the case of anti-PD-1. Prior to assessing combinatorial activity between AB521 and

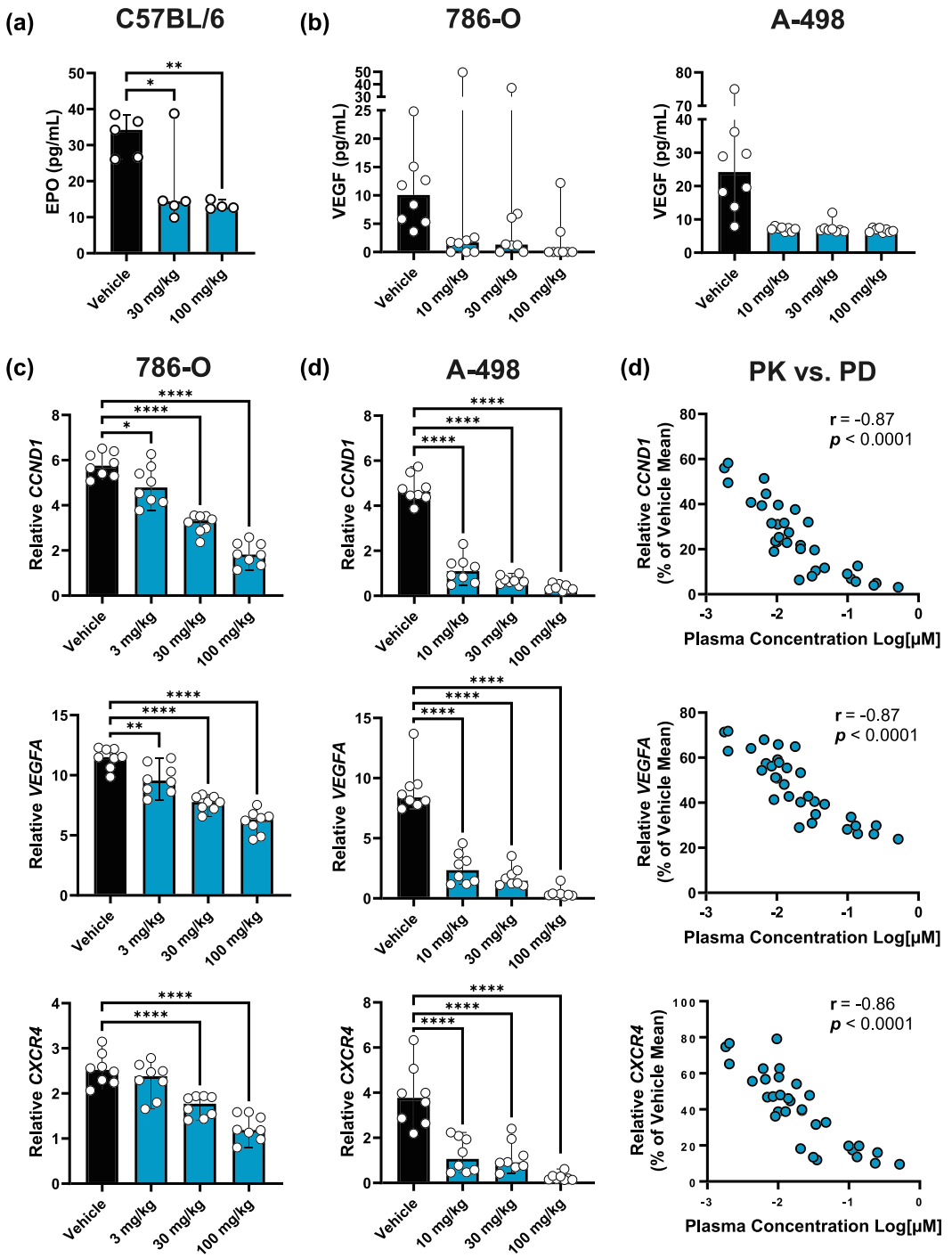

FIGURE 4 AB521 inhibits expression of HIF-2α PD targets in vivo. (a) Mouse EPO levels in plasma of nontumour bearing C57BL/6 mice 8 h after a single oral dose of 30 or 100 mg·kg^{-1} AB521. Results were confirmed in an independent repeat study using the 100 mg·kg^{-1} dose. (b) Human tumour-derived VEGF-A in the plasma of 786-O or A-498-tumour bearing mice 12 h after the final dose of AB521 following 10 days of twice-daily (BID) PO dosing. (c,d) Expression of HIF-2α target genes (*CCND1*, *CXCR4*, *VEGFA*) in tumour lysates harvested from (c) 786-O or (d) A-498 xenograft bearing mice. Tumours were excised 24 h after initiating either a single dose of AB521 (786-O) or two doses given 12 h apart (A-498). (e) Relationship between AB521 plasma concentrations 24 h post-dosing compared with normalised HIF-2α target gene expression. Data collected from mice across two independent studies of 786-O tumour-bearing mice after 1 or 2 doses of 10, 30, or 100 mg·kg^{-1} AB521. Pearson correlation coefficient (*r*) and associated *P*-value are reported. (a–d) Bars and error represent median ± range. Data shown are representative results from at least two independent experiments, unless otherwise indicated, with n > 5 animals per group. Ordinary one-way ANOVA with Dunnett's multiple comparisons test. **P* < 0.05, ***P* < 0.01, ****P* < 0.001, *****P* < 0.0001.

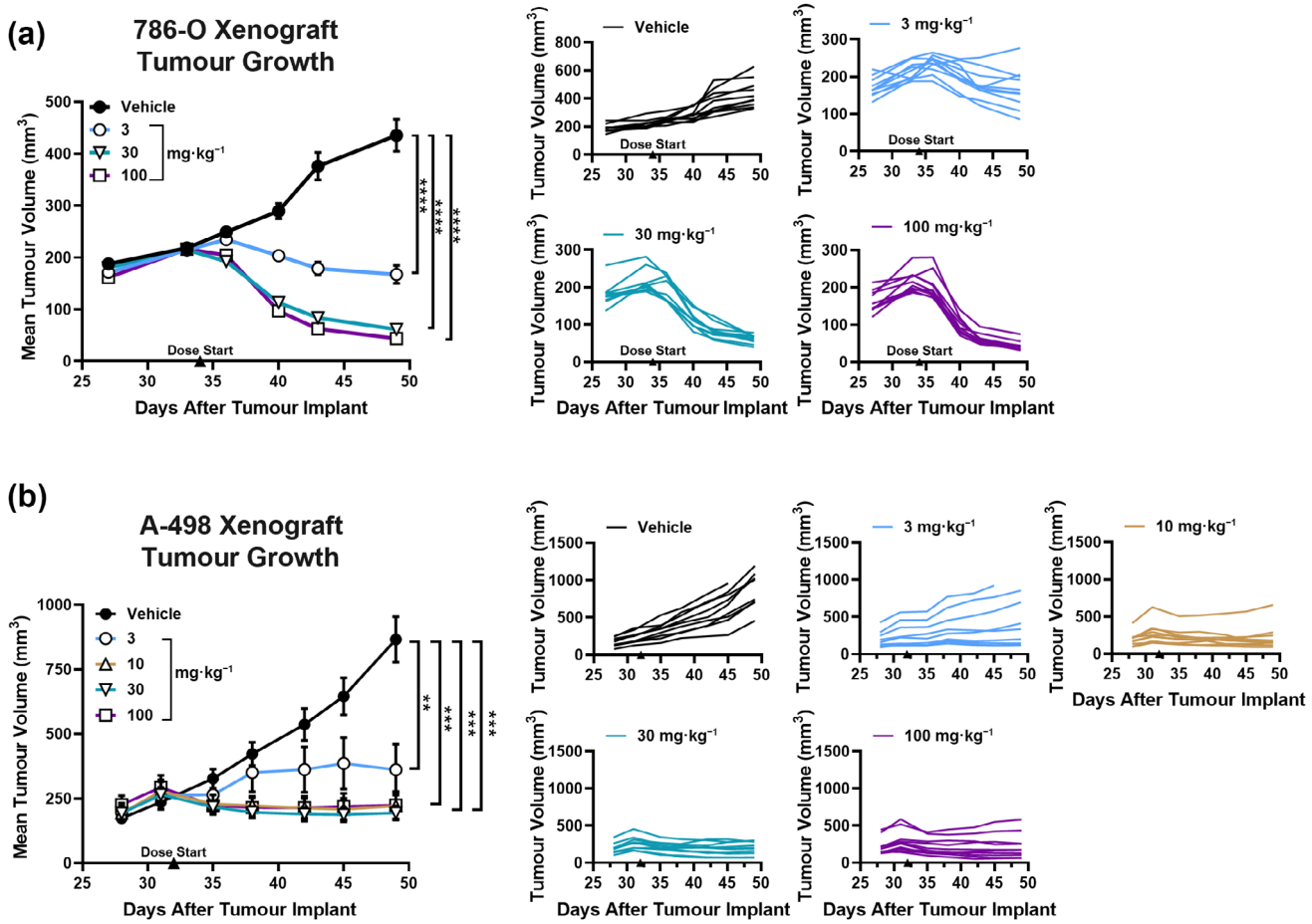

FIGURE 5 AB521 inhibits ccRCC xenograft tumour growth. (a) 786-O and (b) A-498 xenograft tumour growth measurements from mice treated with vehicle or various doses of AB521 PO QD. Summary graphs (left) show mean tumour volume ± SEM (n = 9–10 animals per group), individual tumour growth measurements also are shown (right). The dosing start date is marked on the *x*-axis. Two-way ANOVA with Dunnett's multiple comparisons, significance at study endpoint is denoted, $^{**}P < 0.01$; $^{***}P < 0.001$; $^{****}P < 0.0001$.

anti-PD-1, the impact of HIF-2α inhibition alone on human T-cell activation and functionality was assessed in vitro. Primary human $CD8^+$ T cells showed detectable HIF-1α when cultured in hypoxia, which increased in expression when the cells were activated by anti-CD3/anti-CD28 co-stimulation (Figure S7A), a finding that has been reported previously (Nakamura et al., 2009). By contrast, HIF-2α was detectable only in activated $CD8^+$ T-cells cultured in hypoxia (Figure S7A), and as observed in other cell types (Figures 1c and 2a), HIF-2α protein levels decreased with AB521 treatment (Figure S7A), whereas HIF-1α expression was unaffected. Treatment of $CD8^+$ T cells with AB521 did not alter cytokine secretion or proliferation in normoxic or hypoxic settings (Figure S7B), indicating that HIF-2α inhibition with AB521 did not impede the fundamental behaviour of these cells.

To assess the combinatorial activity of HIF-2α inhibition with an immune-modulating agent, a humanized mouse model was employed. Immunodeficient (NSG-MHC I/II DKO) mice with established A-498 xenograft flank tumours (>200 mm^3) were engrafted with human peripheral blood mononuclear cells (PBMCs). One week after PBMC injection, peripheral blood was collected to monitor human immune cell engraftment, and mice were randomised into four groups based on two variables: human $CD45^+$ engraftment percentage and tumour size (Figures 8a and S8). High levels of engraftment in this model (~20%–30% of live singlets) are not typically observed until 4 weeks post cell injection, hence the modest number of cells in the peripheral blood at day 7. Following randomisation, mice were treated with AB521 and a human PD-1 blocking antibody, zimberelimab (zim), as single agents or in combination. Zim treatment was modestly effective on its own, producing a complete response (defined as no measurable tumour mass) in one of the five treated animals (Figure 8b). By contrast, AB521 as a single agent led to considerable tumour regression in all treated animals, but tumour growth resumed when AB521 treatment was stopped. The combination of AB521 and zim caused more rapid tumour regression than either monotherapy. This combinatorial response from AB521 and zim was sustained in the majority of animals when treatment was halted, with 60% of mice showing a complete response. Together, these results demonstrate that HIF-2α inhibition by AB521 can be effectively combined with other standard of care therapeutic strategies for ccRCC, such as TKIs or checkpoint blockade, to enhance antitumour responses.

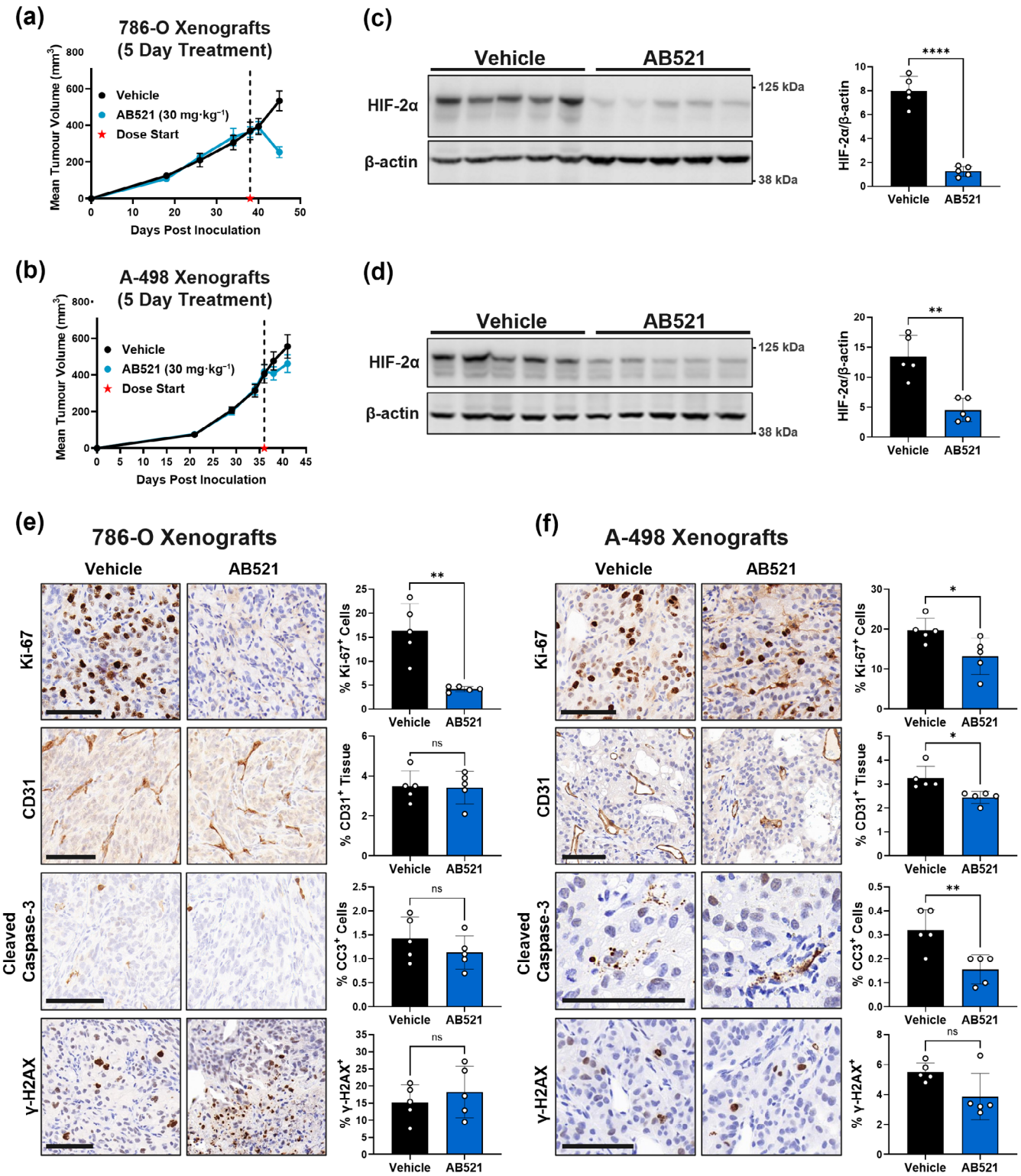

FIGURE 6 Decreased intratumoural HIF-2α and Ki-67 expression in ccRCC xenografts after 5-days of AB521 treatment. Tumour growth curves for (a) 786-O and (b) A-498 xenografts treated for 5 days with AB521 (30 mg·kg^{-1} PO QD) (n = 5 animals per group). Tumours were excised for subsequent immunoblot and tissue staining analyses. (c,d) Immunoblots showing HIF-2α protein expression from tumour lysates of (c) 786-O and (d) A-498 xenografts after 5 days of AB521 treatment. Quantification shown as mean ± SD with each symbol representing an individual mouse tumour sample. (e,f) IHC performed on fixed tumour samples from (e) 786-O and (f) A-498 xenograft tumours staining for Ki-67, CD31, cleaved caspase-3 (CC3), and γ-H2AX. Representative images are shown (scale bar = 100 μm). Quantification shown as mean ± SD with each symbol representing an individual tumour. Unpaired *t*-test with Welch's correction, $^{*}P < 0.05$, $^{**}P < 0.01$, $^{****}P < 0.0001$.

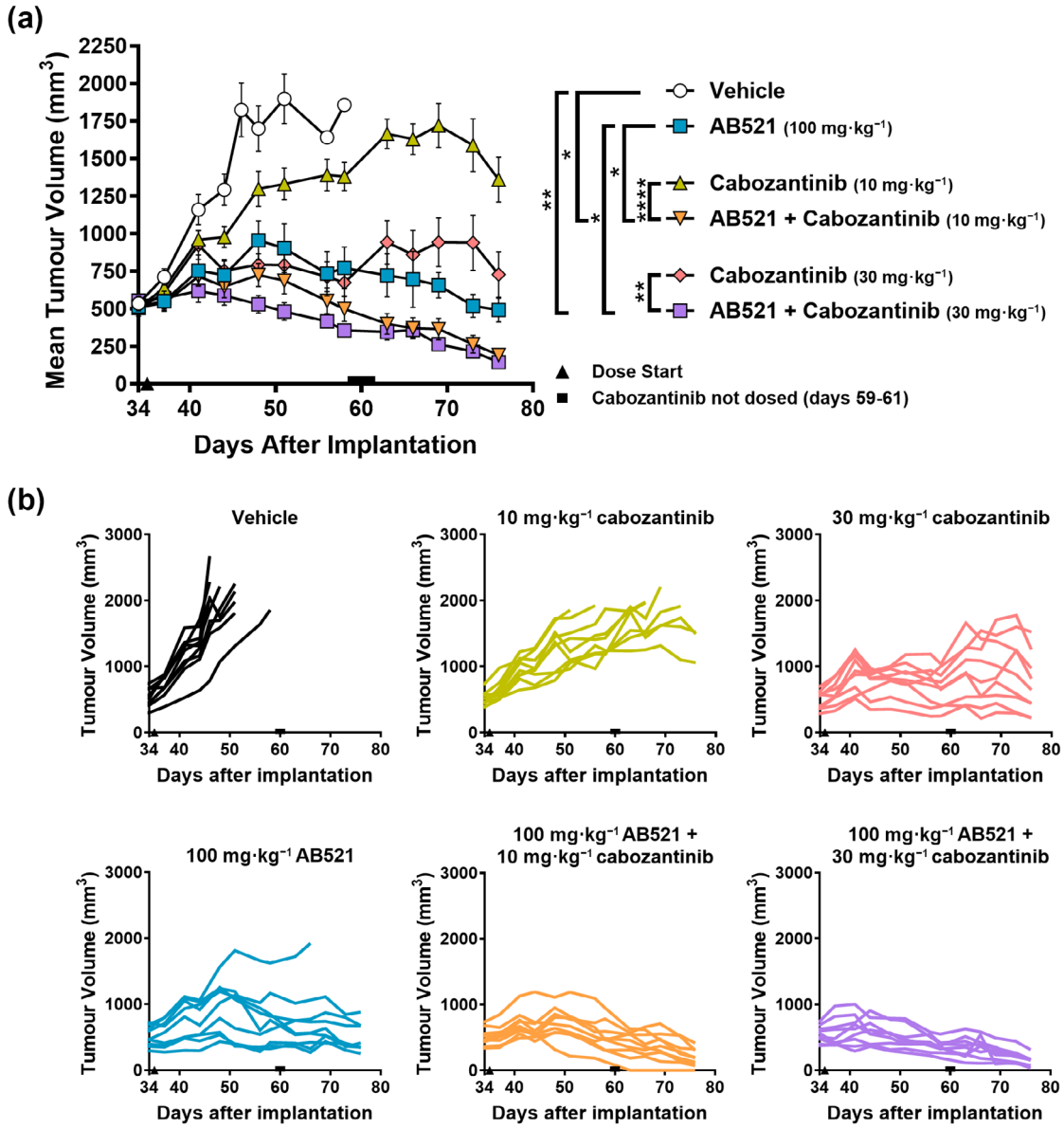

FIGURE 7 AB521 in combination with the TKI cabozantinib enhances A-498 ccRCC xenograft tumour regression. Cabozantinib (10 or 30 mg·kg^{-1}) and/or AB521 (100 mg·kg^{-1}) were delivered orally once daily (PO QD) at the indicated doses to mice bearing established A-498 xenograft tumours. (a) Tumour volume measurements are shown as mean ± standard error of the mean for each treatment group (n = 9/group). Statistical analysis was performed in R using a linear model on square root transformed data with paired *t*-test follow-up with exact Tukey for control of multiple comparisons (vehicle vs. each treatment arm, AB521 vs. each combination group, cabozantinib vs. same concentration combination group). (b) Tumour volume measurements for individual animals are shown. The dosing start date and a break in the cabozantinib treatment (due to compound unavailability) are marked on the *x*-axis. *P < 0.05, **P < 0.01, ****P < 0.0001.

4 | DISCUSSION

The first clinical trial evaluating HIF-2α inhibition as a therapeutic approach to treat ccRCC was initiated in 2014 (NCT02293980) using the first-generation small molecule HIF-2α inhibitor PT2385 (also known as MK-3795). PT2385 was later replaced by a structurally-related second-generation inhibitor, belzutifan (MK-6482/PT2977), featuring improved potency and PK properties (Xu et al., 2019) that is now approved for the treatment of adult patients with pheochromocytoma or paraganglioma (FDA, 2025), advanced RCC (Choueiri et al., 2024) and VHL disease (Jonasch et al., 2021). Statistically significant and clinically meaningful results provided the proof-of-concept for therapeutic targeting of HIF-2α in disease, particularly *VHL* mutation-driven cancers, increasing enthusiasm to develop next-generation HIF-2α inhibitors. Indeed, in addition to AB521, two other small molecule inhibitors of HIF-2α, NKT2152 and **DFF332**, have been tested in Phase 1 clinical trials in patients with ccRCC [NCT05119335 (Jonasch, McGregor, et al., 2024) and NCT04895748 (Pal et al., 2024), respectively], and a tumour-directed siRNA approach has been explored as well [ARO-HIF2/zifcasiran, NCT04169711

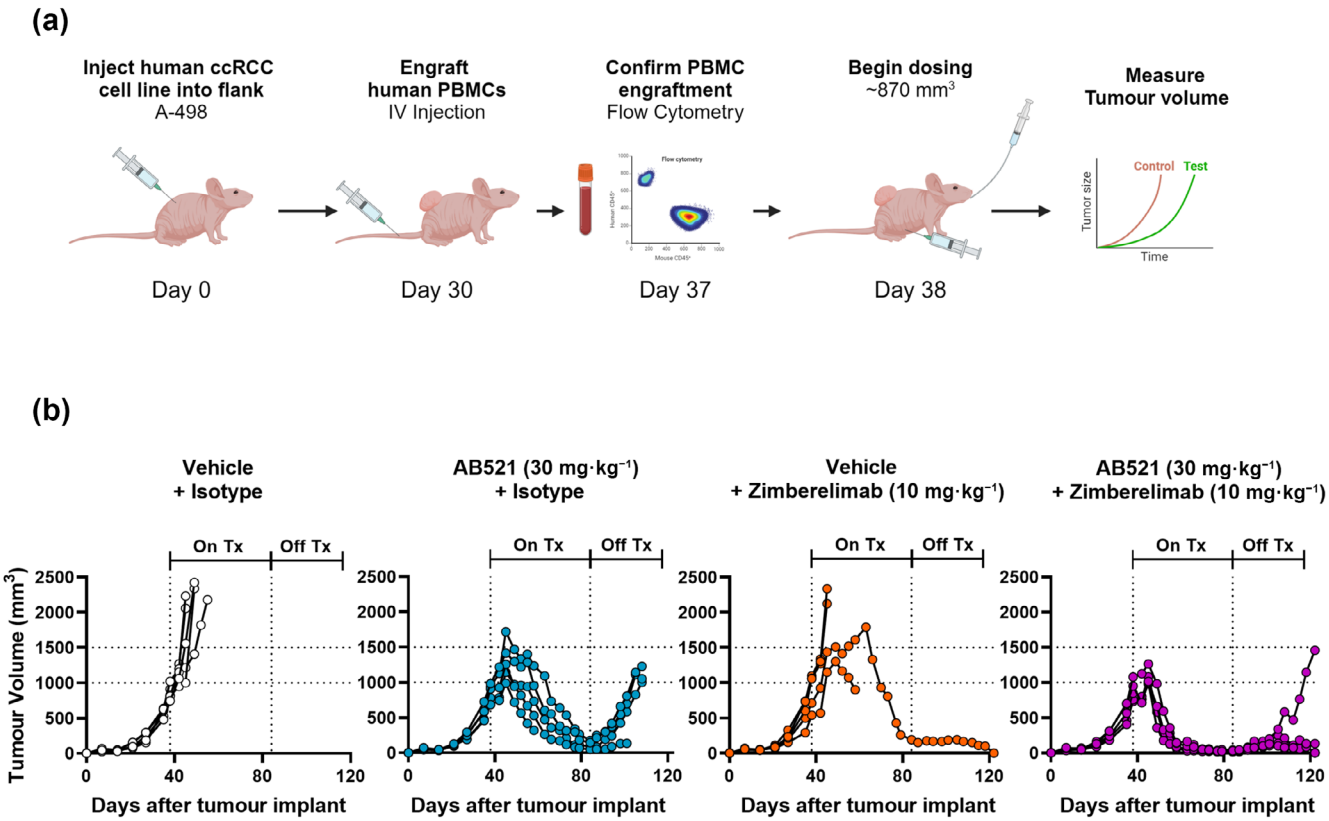

FIGURE 8 AB521 combined with human anti-PD-1 antibody, zimberelimab, enhances tumour control in a humanized PBMC ccRCC tumour growth model. (a) Schematic of the experimental design. NSG-MHCI/II DKO mice were injected with A-498 tumour cells, engrafted by intravenous injection with human PBMCs, and treated with 30 mg·kg^{-1} AB521 orally once daily (PO QD) and/or 10 mg·kg^{-1} anti-PD-1 (zimberelimab) by intraperitoneal injection every 3 days (IP Q3D). (b) Tumour volume measurements from each treatment group (n = 5 animals per group) are shown. Each line represents an individual tumour. The AB521 and zimberelimab treatment start (On Tx) and stop (Off Tx) timepoints are annotated and horizontal dotted lines serve as reference points for comparison across treatment groups.

(Brugarolas et al., 2024)]. Both small molecules exhibited extraordinarily long half-lives (~85 days for DFF332 and ~38 days for NKT2152), negating the utility of dose reductions or drug discontinuations to manage any adverse events. Perhaps for this reason, the DFF332 study was halted before dose optimisation was completed. Development of the HIF-2α-targeting siRNA, ARO-HIF2, also was halted due to low clinical response rate and off-target neurotoxicity (Brugarolas et al., 2024). The clinical success of belzutifan, paired with the unique difficulties hindering the advancement of other HIF-2α inhibitors, provided an opportunity for next-generation HIF-2α inhibitor development. Here, we describe the potential therapeutic benefit of HIF-2α inhibition by a novel, potent, and selective HIF-2α inhibitor, AB521 (casdatifan) (Hardman et al., 2025; Mata et al., 2025), that is suitable for once-daily oral dosing in humans. We note that AB521 was effective at reducing xenograft ccRCC tumour growth, both as a single agent and in combination with relevant TKI or checkpoint inhibitor approaches, and we highlight the potential for HIF-2α inhibition to act on both cancer and non-cancer cells to combat protumourigenic signals and progression.

Hypoxic conditions are frequently present within the heterogenous microenvironment of solid tumours and can influence the behaviour of cancer, stromal, and immune cells (Davis et al., 2022; Steinberger & Eubank, 2023). Inhibition of endogenous HIF-2α-regulated targets by AB521 was demonstrated in in vitro cell systems intended to model cell types and phenotypes present in the TME. In 786-O ccRCC cells, AB521 treatment decreased VEGF protein secretion (Figure 1c), illustrating that inhibition of HIF-2α by AB521 could directly alter endogenous protein expression in an acute time frame, and highlighting the potential for AB521 treatment to rapidly reduce protumourigenic signals within the tumour milieu. In the Hep3B HCC cell line, AB521 selectively inhibited HIF-2α, but not HIF-1α, dependent gene transcription (Figure 2d,e), demonstrating selectivity between these two HIF-α isoforms. Moreover, several reports have identified protumourigenic roles for HIF-2α within stromal and immune cells. The biology of HIF-2α is well studied in the context of angiogenesis, and deletion or knockdown of HIF-2α in endothelial cells can impair tumour vascularization and tumour growth (Skuli et al., 2009; Skuli et al., 2012; Yamashita et al., 2008). HIF-2α expression also has been observed in TAMs within multiple tumour types (Talks et al., 2000), and macrophage expression of HIF-2α was shown to influence macrophage polarization and to promote tumour growth through enhanced TAM migration and tumour site infiltration (Imtiyaz et al., 2010; Takeda et al., 2010). Indeed, using human endothelial cells to model tumour vascular cells and M2-polarised macrophages to

model protumourigenic TAMs, we observed hypoxia-induced transcription of genes involved in angiogenesis, extracellular matrix remodelling, myeloid cell recruitment, and glycolytic metabolism (Figure 3). The expression of these genes was effectively blocked by AB521, underlining the ability of HIF-2α-inhibition to alter the transcriptome of non-malignant cells to dampen protumourigenic signals. Taken together, these findings reinforce the notion that HIF-2α inhibition may target multiple cellular compartments leading to direct changes in cancer cell growth and cross-talk, while also acting on stromal cells to dismantle the protumourigenic microenvironment.

The functional consequences of HIF-2α inhibition on cancer cells was assessed in vitro and showed that AB521 potently inhibited anchorage-independent growth of 786-O cells in a concentration dependent manner (Figure 1e). Similar reliance on HIF-2α for colony formation or spheroid growth has been observed by others (Cho et al., 2016; Cimmino et al., 2016; Hallis et al., 2023; He et al., 2019; Kitajima et al., 2018; Lachance et al., 2014), while cell proliferation in standard 2-D settings was unencumbered by HIF-2α inhibition or loss as observed here and in agreement with published findings (Cho et al., 2016; Kondo et al., 2003; Wallace et al., 2016; Zimmer et al., 2004). Anchorage-independent growth is a hallmark of transformed cells and a trait of tumour-initiating or cancer stem cells (CSCs). Notably, hypoxia and HIF-2α have been shown to promote CSC phenotypes in several settings (Hallis et al., 2023; Myszczyszyn et al., 2015; O'Reilly et al., 2019; Yan et al., 2022), and CSCs are regarded as critical targets for cancer treatment due to their involvement in metastasis, therapy resistance, and post-treatment relapse (Turdo et al., 2019; Zhou et al., 2021). Our results are in line with these findings and support the potential for HIF-2α-inhibition to obstruct the malignant capacity of these difficult-to-target cells.

In vivo characterization of AB521 revealed favourable PK properties and oral bioavailability in mice (Figure S5), enabling once-daily dosing to achieve significant changes in PD markers. PD assessments included monitoring decreases in the serum hormone EPO, a known HIF-2α target that is used clinically to confirm HIF-2α inhibitor activity (Courtney et al., 2017; Courtney et al., 2020; Marathe et al., 2024; Xu et al., 2019), as well as HIF-2α-dependent human genes expressed by the ccRCC xenograft tumours (Figure 4). Importantly, AB521-dependent tumour growth control was observed in our 786-O and A-498 xenograft studies (Figure 5), thus demonstrating efficacy of AB521 as a monotherapy in these models. Acute treatment with AB521 in these models also resulted in a significant reduction of cell proliferation (as measured by Ki-67) within the tumours (Figure 6e), which also has been observed with PT2385 treatment (Wallace et al., 2016). While these studies demonstrate the acute effects of HIF-2α inhibition on ccRCC tumours, it is important to note that components of the tumour microenvironment are missing from these models due to the necessary use of immunocompromised mice. It would be interesting in future studies to evaluate the effects of HIF-2α inhibition in a syngeneic ccRCC model that better recapitulates the totality of the TME, but to date no HIF-2α-sensitive syngeneic models have been developed (Stransky et al., 2024).

Reduction in HIF-2α protein caused by AB521 treatment, both in vitro (Figures 1c and 2a) and in vivo (Figure 6c,d), may ultimately provide a secondary mechanism to block HIF-2α activity beyond disruption of HIF-2α-ARNT dimerisation (Figure 1b). This phenomenon is consistent with past reports profiling other HIF-2α small molecule inhibitors (Cho et al., 2016; Wallace et al., 2016; Yan et al., 2022). The exact reason for this inhibitor-dependent loss of HIF-2α protein is not well understood, although **cycloheximide** experiments demonstrated that PT2385 treatment caused a reduction in HIF-2α protein half-life (Cho et al., 2016), suggesting HIF-2α protein destabilization in the presence of inhibitor. Alternatively, if HIF-2α stability was dependent on an ability to dimerize with ARNT, it would explain why small molecule inhibitors that disrupt the HIF-2α-ARNT complex also cause a reduction in HIF-2α protein. However, no decreases in HIF-2α protein were observed in siRNA and CRISPR/Cas9 ARNT depletion experiments (Figure S1), indicating that ARNT binding does not influence HIF-2α stability or protein levels in these cells. Thus, the precise mechanism(s) by which HIF-2α protein levels are altered in the presence of inhibitor remains an active area of focus.

In vivo HIF-2α inhibition was evaluated in combination with either the standard-of-care TKI (cabozantinib) or an anti-PD-1 antibody (zimberelimab), because these are relevant therapeutic approaches for RCC. Importantly, HIF-2α inhibition did not appear to impede T-cell functionality (Figure S7), lending credence to the idea that this targeted therapy does not pose a risk of impairing immune cell function and may serve as an appealing combination partner for T-cell-modulating agents. We observed improved tumour control with both combination strategies (Figures 7 and 8), supporting the potential advantage of utilizing standard of care approaches in combination with HIF-2α inhibition. These data also revealed that AB521 could be beneficial in instances of sub-optimal TKI inhibition (Figure 7), an important consideration given the need for drug holidays or dose reductions due to adverse effects associated with broad TKI inhibition.

Altogether, the results reported here indicate that AB521 is a potent and selective HIF-2α inhibitor with the ability to effectively impair HIF-2α-dependent gene transcription and cancer cell growth, both as a single agent and in combination with two of the most widely used treatment strategies for ccRCC. AB521, casdatifan, is currently undergoing clinical evaluation for the treatment of ccRCC (NCT05536141).

AUTHOR CONTRIBUTIONS

Experiments were designed, conducted, analysed, and interpreted by Dana Piovesan, Casey G. Mitchell, Lauren Rocha, Patrick G. Schweickert, Cesar Meleza, Alejandra Y. Lopez Espinoza, Bryan Zepeda-Carranza, Wandi S. Zhu, Jaskirat Singh, Martin Ian P. Malgapo, and Kyle R. Northington, with the help of Kelsey E. Sivick and Xiaoning Zhao in experimental design and data interpretation. Rebecca D. Ray performed statistical analyses on mouse tumour studies. This study was supervised by Xiaoning Zhao, Matthew J. Walters, and Kelsey E. Sivick. With the help of others, the overall study was conceptualized by Dana Piovesan, Kelsey E. Sivick, and Matthew

J. Walters. Most of the manuscript was written by Patrick G. Schweickert and Dana Piovesan, with sections contributed by Kelsey E. Sivick and input from Matthew J. Walters. Kenneth V. Lawson contributed to and supervised the discovery of AB521.

ACKNOWLEDGMENTS

This work was funded by Arcus Biosciences. We would like to thank the following groups and individuals: the Pharmacology team at Arcus Biosciences for dedication to and execution of mouse studies, specifically Suan Liu, Ferdie Soriano, Ruben Flores and Janine Kline; the DMPK team at Arcus Biosciences for compound analysis of mouse samples; the Cell Core team at Arcus Biosciences for growing and maintaining cell lines; Research colleagues from Arcus Biosciences for discussion and critical review of the manuscript. The graphic for Figure 8a was created in BioRender: Sivick, K (2025) https://BioRender.com/7khlcjc.

CONFLICT OF INTEREST STATEMENT

PGS, DP, CGM, BZC, WSZ, AYLE, LR, JS, MIPM, CM, KRN, RDR, XZ, KVL, MJW, and KES are currently or were formerly Arcus Biosciences paid employees with stock equity.

DATA AVAILABILITY STATEMENT

The data that support the findings of this study are available from the corresponding author upon reasonable request.

DECLARATION OF TRANSPARENCY AND SCIENTIFIC RIGOUR

This Declaration acknowledges that this paper adheres to the principles for transparent reporting and scientific rigour of preclinical research as stated in the *BJP* guidelines for Natural Products Research, Design and Analysis, Immunoblotting and Immunochemistry, and Animal Experimentation, and as recommended by funding agencies, publishers, and other organizations engaged with supporting research.

ORCID

Patrick G. Schweickert https://orcid.org/0000-0001-9848-9278

REFERENCES

Albanese, A., Daly, L. A., Mennerich, D., Kietzmann, T., & Sée, V. (2021). The role of hypoxia-inducible factor post-translational modifications in regulating its localisation, stability, and activity. *International Journal of Molecular Sciences*, *22*(1), 1–18. https://doi.org/10.3390/ijms22010268

Alexander, S., Fabbro, D., Kelly, E., Mathie, A. A., Peters, J. A., Veale, E. L., Armstrong, J. F., Faccenda, E., Harding, S. D., Davies, J. A., Annett, S., Boison, D., Burns, K. E., Dessauer, C., Gertsch, J., Helsby, N. A., Izzo, A. A., Ostrom, R., Papapetropoulos, A., … Wong, S. S. (2023). The Concise Guide to PHARMACOLOGY 2023/24: Enzymes. *British Journal of Pharmacology*, *180*(Suppl 2), S289–S373.

Alexander, S., Kelly, E., Mathie, A., Peters, J. A., Veale, E. L., Armstrong, J. F., Buneman, O. P., Faccenda, E., Harding, S. D., Spedding, M., Cidlowski, J. A., Fabbro, D., Davenport, A. P., Striessnig, J., Davies, J. A., Ahlers-Dannen, K. E., Alqinyah, M., Arumugam, T. V., Bodle, C., … Zolghadri, Y. (2023). The Concise Guide to PHARMACOLOGY 2023/24: Introduction and other protein targets. *British Journal of Pharmacology*, *180*(Suppl 2), S1–S22.

Alexander, S. P. H., Kelly, E., Mathie, A., Peters, J. A., Veale, E. L., Armstrong, J. F., Faccenda, E., Harding, S. D., Pawson, A. J., Southan, C., Buneman, O. P., Cidlowski, J. A., Christopoulos, A., Davenport, A. P., Fabbro, D., Spedding, M., Striessnig, J., Davies, J. A., Ahlers-Dannen, K. E., … Zolghadri, Y. (2021). The Concise Guide to PHARMACOLOGY 2021/22: Introduction and other protein targets. *British Journal of Pharmacology*, *178*(S1), S1–S26. https://doi.org/10.1111/bph.15537

Alexander, S. P. H., Roberts, R. E., Broughton, B. R. S., Sobey, C. G., George, C. H., Stanford, S. C., Cirino, G., Docherty, J. R., Giembycz, M. A., Hoyer, D., Insel, P. A., Izzo, A. A., Ji, Y., MacEwan, D. J., Mangum, J., Wonnacott, S., & Ahluwalia, A. (2018). Goals and practicalities of immunoblotting and immunohistochemistry: A guide for submission to the British Journal of Pharmacology. *British Journal of Pharmacology*, *175*(3), 407–411. https://doi.org/10.1111/bph.14112

Befani, C., & Liakos, P. (2018). The role of hypoxia-inducible factor-2 alpha in angiogenesis. *Journal of Cellular Physiology*, *233*(12), 9087–9098. https://doi.org/10.1002/JCP.26805

Brugarolas, J., Obara, G., Beckermann, K. E., Rini, B., Lam, E. T., Hamilton, J., Schluep, T., Yi, M., Wong, S., Mao, Z. L., Gamelin, E., & Tannir, N. M. (2024). A first-in-human phase 1 study of a tumor-directed RNA-interference drug against HIF2α in patients with advanced clear cell renal cell carcinoma. *Clinical Cancer Research*, *30*(11), 2402–2411. https://doi.org/10.1158/1078-0432.CCR-23-3029

Büscheck, F., Fraune, C., Simon, R., Kluth, M., Hube-Magg, C., Möller-Koop, C., Sarper, I., Ketterer, K., Henke, T., Eichelberg, C., Dahlem, R., Wilczak, W., Sauter, G., Fisch, M., Eichenauer, T., & Rink, M. (2020). Prevalence and clinical significance of VHL mutations and 3p25 deletions in renal tumor subtypes. *Oncotarget*, *11*(3), 237–249. https://doi.org/10.18632/oncotarget.27428

Chen, W., Hill, H., Christie, A., Kim, M. S., Holloman, E., Pavia-Jimenez, A., Homayoun, F., Ma, Y., Patel, N., Yell, P., Hao, G., Yousuf, Q., Joyce, A., Pedrosa, I., Geiger, H., Zhang, H., Chang, J., Gardner, K. H., Bruick, R. K., … Brugarolas, J. (2016). Targeting renal cell carcinoma with a HIF-2 antagonist. *Nature*, *539*(7627), 112–117. https://doi.org/10.1038/nature19796

Cho, H., Du, X., Rizzi, J. P., Liberzon, E., Chakraborty, A. A., Gao, W., Carvo, I., Signoretti, S., Bruick, R. K., Josey, J. A., Wallace, E. M., & Kaelin, W. G. (2016). On-target efficacy of a HIF-2α antagonist in preclinical kidney cancer models. *Nature*, *539*(7627), 107–111. https://doi.org/10.1038/nature19795

Choueiri, T. K., Bauer, T. M., Papadopoulos, K. P., Plimack, E. R., Merchan, J. R., McDermott, D. F., Michaelson, M. D., Appleman, L. J., Thamake, S., Perini, R. F., Zojwalla, N. J., & Jonasch, E. (2021). Inhibition of hypoxia-inducible factor-2α in renal cell carcinoma with belzutifan: A phase 1 trial and biomarker analysis. *Nature Medicine*, *27*(5), 802–805. https://doi.org/10.1038/s41591-021-01324-7

Choueiri, T. K., Powles, T., Peltola, K., de Velasco, G., Burotto, M., Suarez, C., Ghatalia, P., Iacovelli, R., Lam, E. T., Verzoni, E., Gümüş, M., Stadler, W. M., Kollmannsberger, C., Melichar, B., Venugopal, B., Gross-Goupil, M., Poprach, A., de Santis, M., Schutz, F. A., … LITESPARK-005 Investigators. (2024). Belzutifan versus everolimus for advanced renal-cell carcinoma. *The New England Journal of Medicine*, *391*(8), 710–721. https://doi.org/10.1056/nejmoa2313906

Cimmino, F., Avitabile, M., Pezone, L., Scalia, G., Montanaro, D., Andreozzi, M., Terracciano, L., Iolascon, A., & Capasso, M. (2016). CD55 is a HIF-2α marker with anti-adhesive and pro-invading properties in neuroblastoma. *Oncogene*, *5*, e212. https://doi.org/10.1038/oncsis.2016.20

Conant, D., Hsiau, T., Rossi, N., Oki, J., Maures, T., Waite, K., Yang, J., Joshi, S., Kelso, R., Holden, K., Enzmann, B. L., & Stoner, R. (2022).

Inference of CRISPR edits from sanger trace data. *CRISPR Journal*, *5*(1), 123–130. https://doi.org/10.1089/crispr.2021.0113

Courtney, K. D., Infante, J. R., Lam, E. T., Figlin, R. A., Rini, B. I., Brugarolas, J., Zojwalla, N. J., Lowe, A. M., Wang, K., Wallace, E. M., Josey, J. A., & Choueiri, T. K. (2017). Phase I dose-escalation trial of PT2385, a first-in-class hypoxia-inducible factor-2α antagonist in patients with previously treated advanced clear cell renal cell carcinoma. *Journal of Clinical Oncology*, *36*(9), 867–874. https://doi.org/10.1200/JCO.2017.74.2627

Courtney, K. D., Ma, Y., de Leon, A. D., Christie, A., Xie, Z., Woolford, L., Singla, N., Joyce, A., Hill, H., Madhuranthakam, A. J., Yuan, Q., Xi, Y., Zhang, Y., Chang, J., Fatunde, O., Arriaga, Y., Frankel, A. E., Kalva, S., Zhang, S., … Brugarolas, J. (2020). HIF-2 complex dissociation, target inhibition, and acquired resistance with PT2385, a first-in-class HIF-2 inhibitor, in patients with clear cell renal cell carcinoma. *Clinical Cancer Research*, *26*(4), 793–803. https://doi.org/10.1158/1078-0432.CCR-19-1459

Criscimanna, A., Duan, L. J., Rhodes, J. A., Fendrich, V., Wickline, E., Hartman, D. J., Monga, S. P. S., Lotze, M. T., Gittes, G. K., Fong, G. H., & Esni, F. (2013). PanIN-specific regulation of Wnt signaling by HIF2a during early pancreatic tumorigenesis. *Cancer Research*, *73*(15), 4781–4790. https://doi.org/10.1158/0008-5472.CAN-13-0566

Curtis, M. J., Alexander, S., Cirino, G., Docherty, J. R., George, C. H., Giembycz, M. A., Hoyer, D., Insel, P. A., Izzo, A. A., Ji, Y., MacEwan, D. J., Sobey, C. G., Stanford, S. C., Teixeira, M. M., Wonnacott, S., & Ahluwalia, A. (2018). Experimental design and analysis and their reporting II: Updated and simplified guidance for authors and peer reviewers. *British Journal of Pharmacology*, *175*(7), 987–993. https://doi.org/10.1111/bph.14153

Curtis, M. J., Alexander, S. P. H., Cirino, G., George, C. H., Kendall, D. A., Insel, P. A., Izzo, A. A., Ji, Y., Panettieri, R. A., Patel, H. H., Sobey, C. G., Stanford, S. C., Stanley, P., Stefanska, B., Stephens, G. J., Teixeira, M. M., Vergnolle, N., & Ahluwalia, A. (2022). Planning experiments: Updated guidance on experimental design and analysis and their reporting III. *British Journal of Pharmacology*, *179*(15), 3907–3913. https://doi.org/10.1111/bph.15868

Davis, L., Recktenwald, M., Hutt, E., Fuller, S., Briggs, M., Goel, A., & Daringer, N. (2022). Targeting HIF-2α in the tumor microenvironment: Redefining the role of HIF-2α for solid cancer therapy. *Cancers (Basel)*, *14*(5), 1259. https://doi.org/10.3390/cancers14051259

Downes, N. L., Laham-Karam, N., Kaikkonen, M. U., & Ylä-Herttuala, S. (2018). Differential but complementary HIF1α and HIF2α transcriptional regulation. *Molecular Therapy*, *26*(7), 1735–1745. https://doi.org/10.1016/j.ymthe.2018.05.004

Fallah, J., Brave, M. H., Weinstock, C., Mehta, G. U., Bradford, D., Gittleman, H., Bloomquist, E. W., Charlab, R., Hamed, S. S., Miller, C. P., Dorff, S. E., Chambers, W. A., Mixter, B. D., Dinin, J., Pierce, W. F., Ricks, T. K., Tang, S., Donoghue, M., Pazdur, R., … Beaver, J. A. (2022). FDA approval summary: Belzutifan for von Hippel-Lindau disease–associated tumors. *Clinical Cancer Research*, *28*(22), 4843–4848. https://doi.org/10.1158/1078-0432.CCR-22-1054

FDA. (2025, May). FDA approves belzutifan for pheochromocytoma or paraganglioma. https://www.fda.gov/drugs/resources-information-approved-drugs/fda-approves-belzutifan-pheochromocytoma-or-paraganglioma

Florczyk, U., Czauderna, S., Stachurska, A., Tertil, M., Nowak, W., Kozakowska, M., Poellinger, L., Jozkowicz, A., Loboda, A., & Dulak, J. (2011). Opposite effects of HIF-1α and HIF-2α on the regulation of IL-8 expression in endothelial cells. *Free Radical Biology & Medicine*, *51*(10), 1882–1892. https://doi.org/10.1016/J.FREERADBIOMED.2011.08.023

Foglia, B., Sutti, S., Cannito, S., Rosso, C., Maggiora, M., Autelli, R., Novo, E., Bocca, C., Villano, G., Ramavath, N. N., Younes, R., Tusa, I., Rovida, E., Pontisso, P., Bugianesi, E., Albano, E., & Parola, M. (2022). Hepatocyte-specific deletion of HIF2α prevents NASH-related liver carcinogenesis by decreasing cancer cell proliferation. *Cellular and Molecular Gastroenterology and Hepatology*, *13*(2), 459–482. https://doi.org/10.1016/j.jcmgh.2021.10.002

Fu, X., Pereira, R., De Angelis, C., Veeraraghavan, J., Nanda, S., Qin, L., Cataldo, M. L., Sethunath, V., Mehravaran, S., Gutierrez, C., Chamness, G. C., Feng, Q., O'Malley, B. W., Selenica, P., Weigelt, B., Reis-Filho, J. S., Cohen, O., Wagle, N., Nardone, A., … Schiff, R. (2019). FOXA1 upregulation promotes enhancer and transcriptional reprogramming in endocrine-resistant breast cancer. *Proceedings of the National Academy of Sciences of the United States of America*, *116*(52), 26823–26834. https://doi.org/10.1073/pnas.1911584116

Garcia Garcia, C. J., Huang, Y., Fuentes, N. R., Turner, M. C., Monberg, M. E., Lin, D., Nguyen, N. D., Fujimoto, T. N., Zhao, J., Lee, J. J., Bernard, V., Yu, M., Delahoussaye, A. M., Jimenez Sacarello, I., Caggiano, E. G., Phan, J. L., Deorukhkar, A., Molkentine, J. M., Saur, D., … Taniguchi, C. M. (2022). Stromal HIF2 regulates immune suppression in the pancreatic cancer microenvironment. *Gastroenterology*, *162*(7), 2018–2031. https://doi.org/10.1053/j.gastro.2022.02.024

Geis, T., Döring, C., Popp, R., Grossmann, N., Fleming, I., Hansmann, M. L., Dehne, N., & Brüne, B. (2015). HIF-2alpha-dependent PAI-1 induction contributes to angiogenesis in hepatocellular carcinoma. *Experimental Cell Research*, *331*(1), 46–57. https://doi.org/10.1016/j.yexcr.2014.11.018

Guillen-Quispe, Y. N., Kim, S. J., Saeidi, S., Zhou, T., Zheng, J., Kim, S. H., Fang, X., Chelakkot, C., Rios-Castillo, M. E., Shin, Y. K., & Surh, Y. J. (2023). Oxygen-independent stabilization of HIF-2α in breast cancer through direct interaction with peptidyl-prolyl cis-trans isomerase NIMA-interacting 1. *Free Radical Biology & Medicine*, *207*(July), 296–307. https://doi.org/10.1016/j.freeradbiomed.2023.07.020

Haase, V. H. (2010). Hypoxic regulation of erythropoiesis and iron metabolism. *American Journal of Physiology. Renal Physiology*, *299*(1), F1–F13. https://doi.org/10.1152/ajprenal.00174.2010

Hallis, S. P., Kim, S. K., Lee, J. H., & Kwak, M. K. (2023). Association of NRF2 with HIF-2α-induced cancer stem cell phenotypes in chronic hypoxic condition. *Redox Biology*, *60*(February), 102632. https://doi.org/10.1016/j.redox.2023.102632

Hardman, C., Mailyan, A. K., Mata, G., Beatty, J. W., Drew, S. L., Fournier, J., Kalisiak, J., Rosen, B. R., Epplin, M., Gal, B., Yu, K., Wang, Z., Haelsig, K., Tran, A., Leleti, M. R., Powers, J. P., & Lawson, K. V. (2025). Development of a scalable synthesis of casdatifan (AB521), a potent, selective, clinical-stage inhibitor of HIF-2α. *Organic Process Research & Development*, *5*, 521–535. https://doi.org/10.1021/acs.oprd.4c00497

He, M., Wu, H., Jiang, Q., Liu, Y., Han, L., Yan, Y., Wei, B., Liu, F., Deng, X., Chen, H., Zhao, L., Wang, M., Wu, X., Yao, W., Zhao, H., Chen, J., & Wei, M. (2019). Hypoxia-inducible factor-2α directly promotes BCRP expression and mediates the resistance of ovarian cancer stem cells to adriamycin. *Molecular Oncology*, *13*(2), 403–421. https://doi.org/10.1002/1878-0261.12419

Hoefflin, R., Harlander, S., Abhari, B. A., Peighambari, A., Adlesic, M., Seidel, P., Zodel, K., Haug, S., Göcmen, B., Li, Y., Lahrmann, B., Grabe, N., Heide, D., Boerries, M., Köttgen, A., Heikenwalder, M., & Frew, I. J. (2021). Therapeutic effects of inhibition of sphingosine-1-phosphate signaling in hif-2α inhibitor-resistant clear cell renal cell carcinoma. *Cancers (Basel)*, *13*(19), 1–18. https://doi.org/10.3390/cancers13194801

Imtiyaz, H. Z., Williams, E. P., Hickey, M. M., Patel, S. A., Durham, A. C., Yuan, L. J., Hammond, R., Gimotty, P. A., Keith, B., & Simon, M. C. (2010). Hypoxia-inducible factor 2α regulates macrophage function in mouse models of acute and tumor inflammation. *Journal of Clinical Investigation*, *120*(8), 2699–2714. https://doi.org/10.1172/JCI39506

Jonasch, E., Bauer, T. M., Papadopoulos, K. P., Plimack, E. R., Merchan, J. R., McDermott, D. F., Dror Michaelson, M., Appleman, L. J., Roy, A., Perini, R. F., Liu, Y., & Choueiri, T. K. (2024). Phase I LITESPARK-001 study of belzutifan for advanced solid tumors: Extended 41-month follow-up in the clear cell renal cell carcinoma cohort. *European Journal of Cancer*, *196*(August 2023), 113434. https://doi.org/10.1016/j.ejca.2023.113434

Jonasch, E., Donskov, F., Iliopoulos, O., Rathmell, W. K., Narayan, V. K., Maughan, B. L., Oudard, S., Else, T., Maranchie, J. K., Welsh, S. J., Thamake, S., Park, E. K., Perini, R. F., Linehan, W. M., Srinivasan, R., & MK-6482-004 Investigators. (2021). Belzutifan for renal cell carcinoma in von Hippel-Lindau disease. *The New England Journal of Medicine*, *385*(22), 2036–2046. https://doi.org/10.1056/nejmoa2103425

Jonasch, E., McGregor, B. A., Msaouel, P., Logan, T., Hall, E. T., Bilen, M. A., Falchook, G. S., Shuch, B., Zakharia, Y., Hauke, R., & Gordon, M. (2024). NKT2152, a novel oral HIF-2α inhibitor, in participants (pts) with previously treated advanced clear cell renal carcinoma (accRCC): Preliminary results of a phase I/II study. *Annals of Oncology*, *35*(S2), S1011–S1012. https://doi.org/10.1016/j.annonc.2024.08.1783

Kim, J. W., Tchernyshyov, I., Semenza, G. L., & Dang, C. V. (2006). HIF-1-mediated expression of pyruvate dehydrogenase kinase: A metabolic switch required for cellular adaptation to hypoxia. *Cell Metabolism*, *3*(3), 177–185. https://doi.org/10.1016/j.cmet.2006.02.002

Kitajima, S., Lee, K. L., Fujioka, M., Sun, W., You, J., Chia, G. S., Wanibuchi, H., Tomita, S., Araki, M., Kato, H., & Poellinger, L. (2018). Hypoxia-inducible factor-2 alpha up-regulates CD70 under hypoxia and enhances anchorage-independent growth and aggressiveness in cancer cells present additional targets for the development of novel combinatorial therapeutics. *Oncotarget*, *9*(27), 19123–19135. https://doi.org/10.18632/oncotarget.24919

Kondo, K., Kim, W. Y., Lechpammer, M., & Kaelin, W. G. (2003). Inhibition of HIF2α is sufficient to suppress pVHL-defective tumor growth. *PLoS Biology*, *1*(3), 439–444. https://doi.org/10.1371/journal.pbio.0000083

Lachance, G., Uniacke, J., Audas, T. E., Holterman, C. E., Franovic, A., Payette, J., & Lee, S. (2014). DNMT3a epigenetic program regulates the HIF-2α oxygen-sensing pathway and the cellular response to hypoxia. *Proceedings of the National Academy of Sciences of the United States of America*, *111*(21), 7783–7788. https://doi.org/10.1073/pnas.1322909111

Li, C., Wang, Y., Li, Y., Yu, Q., Jin, X., Wang, X., Jia, A., Hu, Y., Han, L., Wang, J., Yang, H., Yan, D., Bi, Y., & Liu, G. (2018). HIF1α-dependent glycolysis promotes macrophage functional activities in protecting against bacterial and fungal infection. *Scientific Reports*, *8*(1), 1–11. https://doi.org/10.1038/s41598-018-22039-9

Lilley, E., Stanford, S. C., Kendall, D. E., Alexander, S. P. H., Cirino, G., Docherty, J. R., George, C. H., Insel, P. A., Izzo, A. A., Ju, Y., Panettieri, R. A., Sobey, C. G., Stefanska, B., Stephens, G., Teixeira, M., & Ahluwalia, A. (2020). ARRIVE 2.0 and the British Journal of Pharmacology: Updated guidance for 2020. *British Journal of Pharmacology*, *177*(16), 3611–3616. https://doi.org/10.1111/bph.15178

Lou, B., Wei, H., Yang, F., Wang, S., Yang, B., Zheng, Y., Zhu, J., & Yan, S. (2021). Preclinical characterization of GLS-010 (Zimberelimab), a novel fully human anti-PD-1 therapeutic monoclonal antibody for cancer. *Frontiers in Oncology*, *11*(September), 1–10. https://doi.org/10.3389/fonc.2021.736955

Lu, C. W., Lin, S. C., Chien, C. W., Lin, S. C., Lee, C. T., Lin, B. W., Lee, J. C., & Tsai, S. J. (2011). Overexpression of pyruvate dehydrogenase kinase 3 increases drug resistance and early recurrence in colon cancer. *The American Journal of Pathology*, *179*(3), 1405–1414. https://doi.org/10.1016/j.ajpath.2011.05.050

Ma, X., Zhang, H., Xue, X., & Shah, Y. M. (2017). Hypoxia-inducible factor 2 (HIF-2) promotes colon cancer growth by potentiating Yes-associated protein 1 (YAP1) activity. *Journal of Biological Chemistry*, *292*(41), 17046–17056. https://doi.org/10.1074/jbc.M117.805655

Marathe, D. D., Jauslin, P. M., Jan Kleijn, H., De Miranda Silva, C., Chain, A., Abraham, A. K., Kauh, E. A., Liu, Y., Perini, R. F., Alwis, D. P., & Jain, L. (2024). Exposure–response analyses for belzutifan to inform dosing considerations and labeling. *Journal of Clinical Pharmacology*, *64*(10), 1246–1258. https://doi.org/10.1002/jcph.2459

Markham, A. (2021). Zimberelimab: First approval. *Drugs*, *81*(17), 2063–2068. https://doi.org/10.1007/s40265-021-01628-5

Mata, G., Mailyan, A. K., Fournier, J., Beatty, J. W., Leleti, M. R., Powers, J. P., & Lawson, K. V. (2025). Stereodivergent synthesis of the vicinal difluorinated tetralin of casdatifan enabled by Ru-catalyzed transfer hydrogenation. *Organic Letters*, *27*, 833–839. https://doi.org/10.1021/acs.orglett.4c04501

Motzer, R. J., Jonasch, E., Agarwal, N., Alva, A., Baine, M., Beckermann, K., Carlo, M. I., Choueiri, T. K., Costello, B. A., Derweesh, I. H., Desai, A., Ged, Y., George, S., Gore, J. L., Haas, N., Hancock, S. L., Kapur, P., Kyriakopoulos, C., Lam, E. T., … Motter, A. (2022). Kidney cancer, version 3.2022, NCCN clinical practice guidelines in oncology. *Journal of the National Comprehensive Cancer Network*, *20*(1), 71–90. https://doi.org/10.6004/jnccn.2022.0001

Myszczyszyn, A., Czarnecka, A. M., Matak, D., Szymanski, L., Lian, F., Kornakiewicz, A., Bartnik, E., Kukwa, W., Kieda, C., & Szczylik, C. (2015). The role of hypoxia and cancer stem cells in renal cell carcinoma pathogenesis. *Stem Cell Reviews and Reports*, *11*(6), 919–943. https://doi.org/10.1007/s12015-015-9611-y

Nakamura, H., Makino, Y., Okamoto, K., Poellinger, L., Ohnuma, K., Morimoto, C., & Tanaka, H. (2009). TCR engagement increases hypoxia-inducible factor-1α protein synthesis via rapamycin-sensitive pathway under hypoxic conditions in human peripheral T cells. *Journal of Immunology*, *174*(12), 7592–7599. https://doi.org/10.4049/jimmunol.174.12.7592

Nguyen, C. B., Oh, E., Bahar, P., Vaishampayan, U. N., Else, T., & Alva, A. S. (2024). Novel approaches with HIF-2α targeted therapies in metastatic renal cell carcinoma. *Cancers (Basel)*, *16*(3), 1–12. https://doi.org/10.3390/cancers16030601

O'Reilly, D., Johnson, P., & Buchanan, P. J. (2019). Hypoxia induced cancer stem cell enrichment promotes resistance to androgen deprivation therapy in prostate cancer. *Steroids*, *152*(January), 108497. https://doi.org/10.1016/j.steroids.2019.108497

Ortmann, B. M. (2024). Hypoxia-inducible factor in cancer: From pathway regulation to therapeutic opportunity. *BMJ Oncology*, *3*(1), 1–17. https://doi.org/10.1136/bmjonc-2023-000154

Pal, S. K., Tannir, N. M., Grell, P., Gao, X., Kotecha, R. R., Picus, J., de Braud, F. G., Takahashi, S., Wong, A., Suárez, C., Otero, J. A., Kundamal, N., Yang, X., Sharaby, S., Roy, M., Barzaghi-Rinaudo, P., & Albiges, L. (2024). Preliminary safety, pharmacokinetics and clinical activity of DFF332, an oral HIF2α inhibitor, as monotherapy in a phase 1 dose escalation study in patients with advanced clear cell renal cell carcinoma. *Journal of Clinical Oncology*, *42*(16_suppl), 4513. https://doi.org/10.1200/jco.2024.42.16_suppl.4513

Percie du Sert, N., Hurst, V., Ahluwalia, A., Alam, S., Avey, M. T., Baker, M., Browne, W. J., Clark, A., Cuthill, I. C., Dirnagl, U., Emerson, M., Garner, P., Holgate, S. T., Howells, D. W., Karp, N. A., Lazic, S. E., Lidster, K., MacCallum, C. J., Macleod, M., … Würbel, H. (2020). The ARRIVE guidelines 2.0: Updated guidelines for reporting animal research. *PLoS Bilogy*, *18*(7), e3000410. https://doi.org/10.1371/journal.pbio.3000410

Qureshi-Baig, K., Ullmann, P., Haan, S., & Letellier, E. (2017). Tumor-initiating cells: A criTICal review of isolation approaches and new challenges in targeting strategies. *Molecular Cancer*, *16*(1), 1–16. https://doi.org/10.1186/s12943-017-0602-2

Rankin, E. B., Biju, M. P., Liu, Q., Unger, T. L., Rha, J., Johnson, R. S., Simon, M. C., Keith, B., & Haase, V. H. (2007). Hypoxia-inducible factor-2 (HIF-2) regulates hepatic erythropoietin in vivo. *The Journal of Clinical Investigation*, *117*(4), 1068–1077. https://doi.org/10.1172/JCI30117

Schofield, H. K., Tandon, M., Park, M. J., Halbrook, C. J., Ramakrishnan, S. K., Kim, E. C., Shi, J., Omary, M. B., Shah, Y. M., Esni, F., & Pasca di Magliano, M. (2018). Pancreatic HIF2α stabilization leads to chronic pancreatitis and predisposes to mucinous cystic neoplasm. *Cellular and Molecular Gastroenterology and Hepatology*, *5*(2), 169–185.e2. https://doi.org/10.1016/j.jcmgh.2017.10.008

Shay, J. E. S., Imtiyaz, H. Z., Sivanand, S., Durham, A. C., Skuli, N., Hsu, S., Mucaj, V., Eisinger-Mathason, T. S. K., Krock, B. L., Giannoukos, D. N., & Simon, M. C. (2014). Inhibition of hypoxia-inducible factors limits tumor progression in a mouse model of colorectal cancer. *Carcinogenesis*, *35*(5), 1067–1077. https://doi.org/10.1093/carcin/bgu004

Shinojima, T., Oya, M., Takayanagi, A., Mizuno, R., Shimizu, N., & Murai, M. (2007). Renal cancer cells lacking hypoxia inducible factor (HIF)-1α expression maintain vascular endothelial growth factor expression through HIF-2α. *Carcinogenesis*, *28*(3), 529–536. https://doi.org/10.1093/carcin/bgl143

Skuli, N., Liu, L., Runge, A., Wang, T., Yuan, L., Patel, S., Iruela-Arispe, L., Simon, M. C., & Keith, B. (2009). Endothelial deletion of hypoxia-inducible factor-2α (HIF-2α) alters vascular function and tumor angiogenesis. *Blood*, *114*(2), 469–477. https://doi.org/10.1182/blood-2008-12-193581

Skuli, N., Majmundar, A. J., Krock, B. L., Mesquita, R. C., Mathew, L. K., Quinn, Z. L., Runge, A., Liu, L., Kim, M. N., Liang, J., Schenkel, S., Yodh, A. G., Keith, B., & Simon, M. C. (2012). Endothelial HIF-2α regulates murine pathological angiogenesis and revascularization processes. *Journal of Clinical Investigation*, *122*(4), 1427–1443. https://doi.org/10.1172/JCI57322

Smythies, J. A., Sun, M., Masson, N., Salama, R., Simpson, P. D., Murray, E., Neumann, V., Cockman, M. E., Choudhry, H., Ratcliffe, P. J., & Mole, D. R. (2019). Inherent DNA -binding specificities of the HIF-1α and HIF-2α transcription factors in chromatin. *EMBO Reports*, *20*(1), 1–17. https://doi.org/10.15252/embr.201846401

Sowter, H. M., Raval, R. R., Moore, J. W., Ratcliffe, P. J., & Harris, A. L. (2003). Erratum: Predominant role of hypoxia-inducible transcription factor (Hif)-1α versus Hif-2α in regulation of the transcriptional response to hypoxia (Cancer Research (October 1, 2003)(6130-6134)). *Cancer Research*, *63*(23), 8562.

Steinberger, K. J., & Eubank, T. D. (2023). The underexplored landscape of hypoxia-inducible factor 2 alpha and potential roles in tumor macrophages: A review. *Oxygen*, *3*(1), 45–76. https://doi.org/10.3390/oxygen3010005

Stransky, L. A., Gao, W., Schmidt, L. S., Bi, K., Ricketts, C. J., Ramesh, V., James, A., Difilippantonio, S., Ileva, L., Kalen, J. D., Karim, B., Jeon, A., Morgan, T., Warner, A. C., Turan, S., Unite, J., Tran, B., Choudhari, S., Zhao, Y., … Kaelin, W. G. Jr. (2024). Toward a CRISPR- based mouse model of Vhl- deficient clear cell kidney cancer: Initial experience and lessons learned. *Proceedings of the National Academy of Sciences*, *121*(41), e2408549121. https://doi.org/10.1073/pnas.2408549121

Stransky, L. A., Vigeant, S. M., Huang, B., West, D., Denize, T., Walton, E., Signoretti, S., & Kaelin, W. G. Jr. (2022). Sensitivity of VHL mutant kidney cancers to HIF2 inhibitors does not require an intact p53 pathway. *Proceedings of the National Academy of Sciences of the United States of America*, *119*(14), e2120403119. https://doi.org/10.1073/pnas.2120403119

Takeda, N., O'Dea, E. L., Doedens, A., Kim, J. W., Weidemann, A., Stockmann, C., Asagiri, M., Simon, M. C., Hoffmann, A., & Johnson, R. S. (2010). Differential activation and antagonistic function of HIF-α isoforms in macrophages are essential for NO homeostasis. *Genes & Development*, *24*(5), 491–501. https://doi.org/10.1101/gad.1881410

Talks, K. L., Turley, H., Gatter, K. C., Maxwell, P. H., Pugh, C. W., Ratcliffe, P. J., & Harris, A. L. (2000). The expression and distribution of the hypoxia-inducible factors HIF-1α and HIF-2α in normal human tissues, cancers, and tumor-associated macrophages. *The American Journal of Pathology*, *157*(2), 411–421. https://doi.org/10.1016/S0002-9440(10)64554-3

Toledo, R. A., Jimenez, C., Armaiz-Pena, G., Arenillas, C., Capdevila, J., & Dahia, P. L. M. (2023). Hypoxia-inducible factor 2 alpha (HIF2α) inhibitors: Targeting genetically driven tumor hypoxia. *Endocrine Reviews*, *44*(2), 312–322. https://doi.org/10.1210/endrev/bnac025

Turdo, A., Veschi, V., Gaggianesi, M., Chinnici, A., Bianca, P., Todaro, M., & Stassi, G. (2019). Meeting the challenge of targeting cancer stem cells. *Frontiers in Cell and Development Biology*, *7*(February), 1–16. https://doi.org/10.3389/fcell.2019.00016

U.S. Food & Drug Administration. (2023). FDA approves belzutifan for advanced renal cell carcinoma. Published 2023. Accessed January 7, 2024. https://www.fda.gov/drugs/resources-information-approved-drugs/fda-approves-belzutifan-advanced-renal-cell-carcinoma

Wallace, E. M., Rizzi, J. P., Han, G., Wehn, P. M., Cao, Z., du, X., Cheng, T., Czerwinski, R. M., Dixon, D. D., Goggin, B. S., Grina, J. A., Halfmann, M. M., Maddie, M. A., Olive, S. R., Schlachter, S. T., Tan, H., Wang, B., Wang, K., Xie, S., … Josey, J. A. (2016). A small-molecule antagonist of HIF2α is efficacious in preclinical models of renal cell carcinoma. *Cancer Research*, *76*(18), 5491–5500. https://doi.org/10.1158/0008-5472.CAN-16-0473

Wehn, P. M., Rizzi, J. P., Dixon, D. D., Grina, J. A., Schlachter, S. T., Wang, B., Xu, R., Yang, H., du, X., Han, G., Wang, K., Cao, Z., Cheng, T., Czerwinski, R. M., Goggin, B. S., Huang, H., Halfmann, M. M., Maddie, M. A., Morton, E. L., … Wallace, E. M. (2018). Design and activity of specific hypoxia-inducible factor-2α (HIF-2α) inhibitors for the treatment of clear cell renal cell carcinoma: Discovery of clinical candidate (S)-3-((2,2-Difluoro-1-hydroxy-7-(methylsulfonyl)-2,3-dihydro-1H-inden-4-yl)oxy)-5-fluoro. *Journal of Medicinal Chemistry*, *61*(21), 9691–9721. https://doi.org/10.1021/acs.jmedchem.8b01196

White, J. R., Harris, R. A., Lee, S. R., Craigon, M. H., Binley, K., Price, T., Beard, G. L., Mundy, C. R., & Naylor, S. (2004). Genetic amplification of the transcriptional response to hypoxia as a novel means of identifying regulators of angiogenesis. *Genomics*, *83*(1), 1–8. https://doi.org/10.1016/S0888-7543(03)00215-5

Wu, D., Su, X., Lu, J., Li, S., Hood, B. L., Vasile, S., Potluri, N., Diao, X., Kim, Y., Khorasanizadeh, S., & Rastinejad, F. (2019). Bidirectional modulation of HIF-2 activity through chemical ligands. *Nature Chemical Biology*, *15*(4), 367–376. https://doi.org/10.1038/s41589-019-0234-5

Xu, R., Wang, K., Rizzi, J. P., Huang, H., Grina, J. A., Schlachter, S. T., Wang, B., Wehn, P. M., Yang, H., Dixon, D. D., Czerwinski, R. M., du, X., Ged, E. L., Han, G., Tan, H., Wong, T., Xie, S., Josey, J. A., & Wallace, E. M. (2019). 3-[(1 S,2 S,3 R)-2,3-Difluoro-1-hydroxy-7-methylsulfonylindan-4-yl]oxy-5-fluorobenzonitrile (PT2977), a hypoxia-inducible factor 2α (HIF-2α) inhibitor for the treatment of clear cell renal cell carcinoma. *Journal of Medicinal Chemistry*, *62*(15), 6876–6893. https://doi.org/10.1021/acs.jmedchem.9b00719

Xue, X., Ramakrishnan, S. K., Weisz, K., Triner, D., Xie, L., Attili, D., Pant, A., Győrffy, B., Zhan, M., Carter-Su, C., Hardiman, K. M., Wang, T. D., Dame, M. K., Varani, J., Brenner, D., Fearon, E. R., & Shah, Y. M. (2016). Iron uptake via DMT1 integrates cell cycle with JAK-STAT3 signaling to promote colorectal tumorigenesis. *Cell Metabolism*, *24*(3), 447–461. https://doi.org/10.1016/j.cmet.2016.07.015

Xue, X., Taylor, M., Anderson, E., Hao, C., Qu, A., Greenson, J. K., Zimmermann, E. M., Gonzalez, F. J., & Shah, Y. M. (2012). Hypoxia-inducible factor-2α activation promotes colorectal cancer progression by dysregulating iron homeostasis. *Cancer Research*, *72*(9), 2285–2293. https://doi.org/10.1158/0008-5472.CAN-11-3836

Yakes, F. M., Chen, J., Tan, J., Yamaguchi, K., Shi, Y., Yu, P., Qian, F., Chu, F., Bentzien, F., Cancilla, B., Orf, J., You, A., Laird, A. D., Engst, S., Lee, L., Lesch, J., Chou, Y. C., & Joly, A. H. (2011). Cabozantinib

(XL184), a novel MET and VEGFR2 inhibitor, simultaneously suppresses metastasis, angiogenesis, and tumor growth. *Molecular Cancer Therapeutics*, *10*(12), 2298–2308. https://doi.org/10.1158/1535-7163.MCT-11-0264

Yamashita, T., Ohneda, K., Nagano, M., Miyoshi, C., Kaneko, N., Miwa, Y., Yamamoto, M., Ohneda, O., & Fujii-Kuriyama, Y. (2008). Hypoxia-inducible transcription factor-2α in endothelial cells regulates tumor neovascularization through activation of ephrin A1. *Journal of Biological Chemistry*, *283*(27), 18926–18936. https://doi.org/10.1074/jbc.M709133200

Yan, Y., He, M., Zhao, L., Wu, H., Zhao, Y., Han, L., Wei, B., Ye, D., Lv, X., Wang, Y., Yao, W., Zhao, H., Chen, B., Jin, Z., Wen, J., Zhu, Y., Yu, T., Jin, F., & Wei, M. (2022). A novel HIF-2α targeted inhibitor suppresses hypoxia-induced breast cancer stemness via SOD2-mtROS-PDI/GPR78-UPRER axis. *Cell Death and Differentiation*, *29*(9), 1769–1789. https://doi.org/10.1038/s41418-022-00963-8

Young, A. C., Craven, R. A., Cohen, D., Taylor, C., Booth, C., Harnden, P., Cairns, D. A., Astuti, D., Gregory, W., Maher, E. R., Knowles, M. A., Joyce, A., Selby, P. J., & Banks, R. E. (2009). Analysis of VHL gene alterations and their relationship to clinical parameters in sporadic conventional renal cell carcinoma. *Clinical Cancer Research*, *15*(24), 7582–7592. https://doi.org/10.1158/1078-0432.CCR-09-2131

Yuan, X., Ruan, W., Bobrow, B., Carmeliet, P., & Eltzschig, H. K. (2024). Targeting hypoxia-inducible factors: Therapeutic opportunities and challenges. *Nature Reviews. Drug Discovery*, *23*(3), 175–200. https://doi.org/10.1038/s41573-023-00848-6

Zhou, H. M., Zhang, J. G., Zhang, X., & Li, Q. (2021). Targeting cancer stem cells for reversing therapy resistance: Mechanism, signaling, and prospective agents. *Signal Transduction and Targeted Therapy*, *6*(1), 62. https://doi.org/10.1038/s41392-020-00430-1

Zimmer, M., Doucette, D., Siddiqui, N., & Iliopoulos, O. (2004). Inhibition of hypoxia-inducible factor is sufficient for growth suppression of VHL−/− tumors. *Molecular Cancer Research*, *2*(2), 89–95. https://doi.org/10.1158/1541-7786.89.2.2

SUPPORTING INFORMATION

Additional supporting information can be found online in the Supporting Information section at the end of this article.

How to cite this article: Schweickert, P. G., Piovesan, D., Mitchell, C. G., Zepeda-Carranza, B., Zhu, W. S., Lopez Espinoza, A. Y., Rocha, L., Singh, J., Malgapo, M. I. P., Meleza, C., Northington, K. R., Ray, R. D., Zhao, X., Lawson, K. V., Walters, M. J., & Sivick, K. E. (2025). Casdatifan (AB521) is a novel and potent allosteric small molecule inhibitor of protumourigenic HIF-2α dependent transcription. *British Journal of Pharmacology*, 1–21. https://doi.org/10.1111/bph.70075